



Persistent warming and anomalous biogeochemical signatures observed in the Northern Tropical Pacific Ocean during 2013–2020

Feng Tian^{1,3} · Rong-Hua Zhang^{2,3,4}

Received: 5 October 2023 / Accepted: 1 March 2024

© The Author(s), under exclusive licence to Springer-Verlag GmbH Germany, part of Springer Nature 2024

Abstract

During 2013–2020, the northern tropical Pacific Ocean (NTPO, 5° N–20° N) experienced a persistent surface warming of over 0.5 °C. This warming was accompanied by a consecutively low surface chlorophyll (SChl). Here, we combined observations with ocean general circulation model experiments to determine how the interplays between the North Pacific meridional mode (NPMM) and multi-year El Niño events jointly led to this persistent surface warming. The warm phase of NPMM (+) excited an anticyclonic circulation in the NTPO, which caused surface warming and enhanced the upper-ocean stratification in the western sector (160° E–150° W) and also deepened the thermocline in the eastern sector (150° W–110° W), resulting in a widespread decline in SChl. The NPMM (+) also triggered El Niño events during the subsequent winter, further decreasing the negative SChl anomalies by weakening the surface ocean current. Subsequently, two persistent El Niño events happened in succession (2014–2016 and 2018–2020), which acted to accelerate the decline in SChl by 2020. These results help to illustrate the effects of extratropical-tropical interactions on the compound physical-biological extremes under the global warming scenario.

1 Introduction

The global ocean has experienced substantial warming since the 1950s at least, exerting a far-reaching influence on the earth's climate and marine ecosystems (Doney et al. 2012; Smale et al. 2019; Cheng et al. 2022; Duan et al. 2023). Concurrent with long-term persistent warming, extreme weather, and biogeochemical events frequently occur in many parts of the world, such as extreme El Niño events, Indian Ocean Dipole, marine heatwaves (MHWs), and so on (Cai et al. 2014, 2021; Gruber et al. 2021). A series of

high-impact MHWs have been recorded in the global oceans and attract much more attention in the scientific community (e.g., Northeastern Pacific during 2013–2014 (Di Lorenzo and Mantua 2016), Tasman Sea (Oliver et al. 2017) and tropical Indian Ocean during 2015–2016 (Zhan et al. 2023), and North Pacific in 2019 (Amaya et al. 2020)). These MHWs event exerts a series of chain reactions and profound influences on the marine ecosystem, such as harmful algal bloom, rapid dieback of kelp forests, coral bleaching and mortality (Smith et al. 2023).

For example, during 2013–2014 and 2019, two MHWs events (also called Blob 1.0 and 2.0) occurred in the northeast Pacific, with maximum warm anomaly exceeding 2.5 °C relative to climatology mean (Di Lorenzo and Mantua 2016; Schmeisser et al. 2019; Amaya et al. 2020; Chen et al. 2023). These two Blob events were followed by a super El Niño (Niño 3.4 index > 3.0 °C) during 2015–2016 and a moderate El Niño (Niño 3.4 index > 1.0 °C) during 2018–2019 in the central-eastern equatorial Pacific (Ding et al. 2022; Guan et al. 2023). Concurrent with these extremely warm events in the Pacific (Liu et al. 2023), the northern tropical Pacific (NTPO, 5°–20° N) also exhibited persistent warming from 2013 to 2020, which was not well recognized, and the related physical mechanism and ecosystem responses remained unclear (Fig. 1a). For instance, surface chlorophyll

✉ Feng Tian
tianfeng@qdio.ac.cn

✉ Rong-Hua Zhang
rzhang@nuist.edu.cn

¹ Key Laboratory of Ocean Observation and Forecasting, Key Laboratory of Ocean Circulation and Waves, Chinese Academy of Sciences, Qingdao 266071, China

² School of Marine Sciences, Nanjing University of Information Science and Technology, Nanjing 210044, China

³ Laoshan Laboratory, Qingdao 266237, China

⁴ University of Chinese Academy of Sciences, Beijing 10029, China

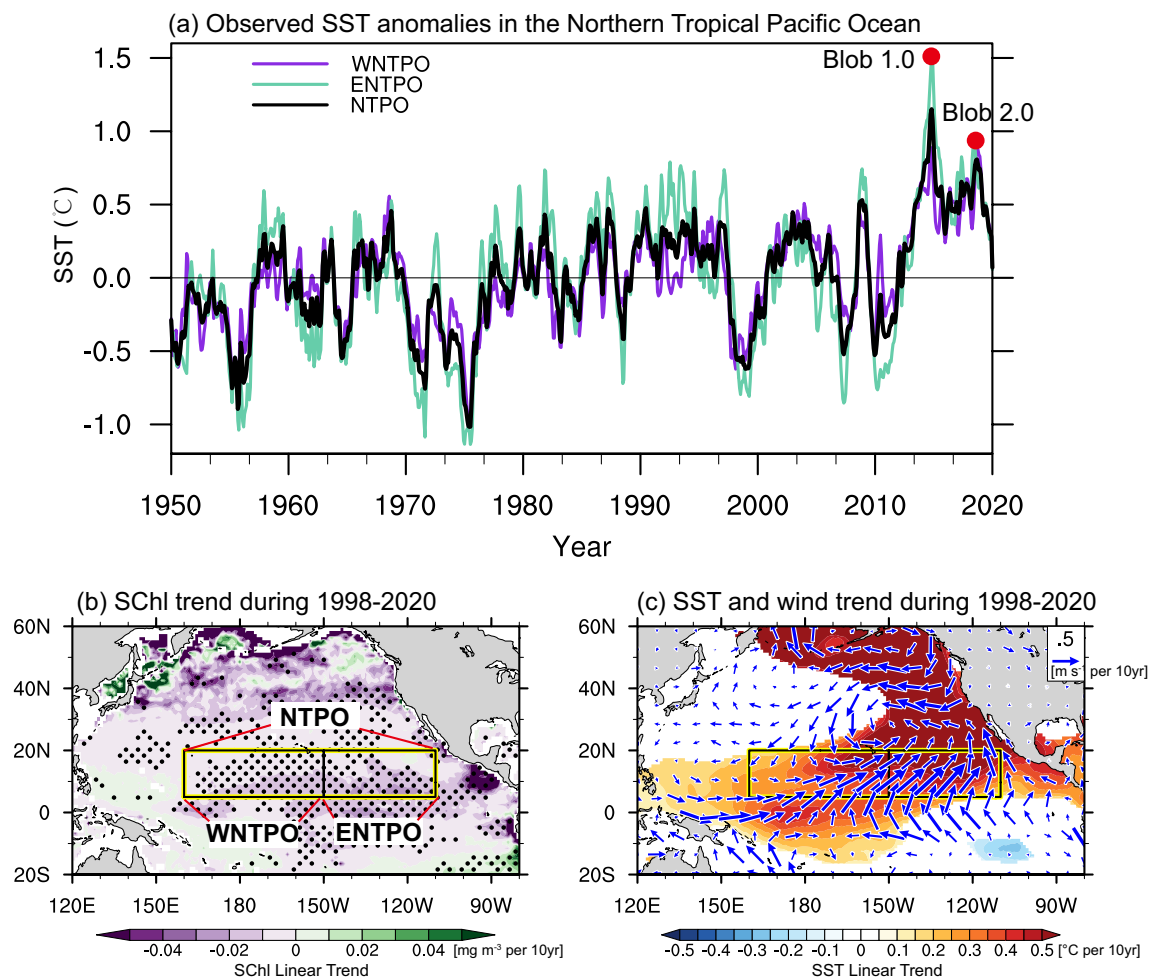


Fig. 1 **a** Time series of monthly-mean SST anomalies averaged over the NTPO. **b** Linear trend in surface chlorophyll and **c** SST (shaded) and surface wind (vector) during 1998–2020, respectively. Statistically significant trends at the 90% level are indicated by stippling in **b**, **c** (only shown for SST). Red dots in **a** denote two Blob events,

as Amaya (2019) indicated. Black rectangles in **b**, **c** show the NTPO area (160° E– 110° W, 5° N– 20° N), WNTPO area (160° E– 150° W, 5° N– 20° N), and ENTPO area (150° W– 110° W, 5° N– 20° N), respectively. The SST data are from the NOAA ERSSTv5 and SchI data are from the GlobColor project

(SchI) exhibited a remarkably decreasing trend in the NTPO associated with persistent SST warming during 2013–2020 (Fig. 1b, c). Given that the NTPO is located between the subtropical North Pacific and the equatorial Pacific, its persistent warming and decreasing SchI events may be related to the interactions between the extra-tropics and tropical oceans with their combined effect on the marine ecosystem.

In the equatorial Pacific, interannual variability in SchI is dominated by ENSO, which exerts significant dynamical and thermodynamic effects, consequently controlling the three-dimensional distribution of nutrients (Chavez et al. 1998). During El Niño, for example, the deepening of the thermocline in the eastern equatorial Pacific weakens the subsurface cold water entrained into the mixed layer and contributes to surface warming. Correspondingly, subsurface nutrient-rich water is hardly transported into the euphotic zone due to the deepening of nitracline (analogous to the

thermocline) (Murtugudde et al. 1999). In the central-western equatorial Pacific, the zonal migration of the warm pool leads to remarkable changes in temperature, salinity, nutrients, and chlorophyll (Maes 2000; Christian et al. 2001). Thus, the zonal advection is widely recognized as the primary driver for interannual variability in SchI (Turk et al. 2011; Radenac et al. 2012; Messié and Chavez 2013; Shi and Wang 2014; Lee et al. 2014). In the western sector of the NTPO, enhanced eastward countercurrents (NECC) drive the advection of oligotrophic warm pool waters within 8 – 10° N and subsequently results in negative anomalies in SchI (Radenac et al. 2012). Additionally, the persistently negative chlorophyll anomalies can be associated with the decay phase of El Niño when the SchI quickly recovers from negative anomalies in the equatorial Pacific (Park et al. 2011). Messié and Chavez (2013) also noted that the spatial pattern of the second mode in SchI derived from

empirical orthogonal function (EOF) was also associated with the North Pacific Gyre Oscillation (NPGO). Therefore, SChl anomalies in the NTPO can be induced by the extratropical climate modes, like NPGO, PDO, or North Pacific Meridional Mode (NPMM).

In the North Pacific, NPMM is a dominant mode of the coupled ocean–atmosphere variability, and its associated SST anomalies (SSTAs) usually precedes El Niño and La Niña events. NPMM is mainly initiated by the atmospheric variability in the North Pacific, with positive subtropical SSTAs being maintained by southwesterly surface wind anomalies associated with negative sea level pressure in the subtropical Pacific. This warm SSTA signature extends southwestwards towards the equator via a wind–evaporation–SST (WES) feedback during the boreal spring. Subsequently, the NPMM-related spatial pattern exhibits warm SSTAs in the subtropical Pacific and cold SSTAs in the eastern tropical Pacific, which induces surface westerly wind anomalies in the western-central tropical Pacific. Consequently, an El Niño event gradually develops under the westerly wind anomalies forcing (Vimont et al. 2003; Chang et al. 2007; Amaya 2019; Jia et al. 2021).

So far, the interactions between the tropical and extratropical oceans have been well investigated (Ding et al. 2022). However, as a transitional zone for the interaction, the dynamics of the NTPO and its biogeochemical signature still need to be clarified. Inspired by the persistent warming and low chlorophyll in the NTPO during 2013–2020 (Figs. 1 and 2a), we further examine the dynamical mechanism of persistent warming and its biological effects during this special period and investigate the remote impact on the tropical Pacific from the North Pacific warm blob events.

This paper is organized as follows. Section 2 introduces the data used, model experiments, and methods. Section 3 presents observed characteristics in the NTPO during the persistent period (2013–2020). Dynamical processes and climate modes responsible for persistent anomalies are shown in Sect. 4 and 5, respectively. Discussions and summaries are given in Sects. 6 and 7, respectively.

2 Data and Method

2.1 Data

In this study, we adopt a series of observational and reanalysis products from various monthly mean physical and biological fields during 1998–2020. The seasonal cycle is removed from all fields and time series to focus on interannual anomalies. SChl fields are from merged ocean color data supplied by the GlobColor Project, with the horizontal resolution being 100 km (Maritorena et al. 2010). SST data are obtained from ERSSTv5 provided by the NOAA/NCEI

(Huang et al. 2017). Sea surface height (SSH) and geostrophic current fields are taken from the CMEMS. Surface wind data are from ECMWF/ERA5 (Hersbach et al. 2020). In addition, potential temperature and salinity are from Met Office EN4 objective analysis (Good et al. 2013). Available net primary production (NPP) data during 2003–2020 are obtained from the Ocean Productivity at Oregon State University website. To further analyze the specific mechanisms, we perform heat budget analysis by adopting the Global Ocean Data Assimilation System (GODAS) developed at the National Centers for Environmental Prediction (NCEP) reanalysis data (Behringer 2007). The GODAS is based on a quasi-global configuration of the GFDL MOM.v3. The model domain extends from 75° S to 65° N and has a resolution of 1° by 1° and enhances to 1/3° in the meridional direction within 10° of the equator. The GODAS assimilates temperature profiles and, as another new feature, assimilates synthetic salinity profiles as well.

The Copernicus Marine Environment Monitoring Service (CMEMS) biogeochemical hindcast data are adopted to elucidate the responses of nutrients to persistent warming events. The CMEMS biogeochemical hindcast simulation is produced by the Mercator-Ocean (Toulouse, France), which is based on the PISCES biogeochemical model (Aumont et al. 2015; Aumont and Bopp 2006) and is available at the CMEMS website. Given that this product is an offline simulation under the PISCES model, the physical variables for the driven PISCES model are the output from GLORYS2V4-FREE output, which is based on the NEMO3.6 ocean model without data assimilation (Madec 2014). The ocean model configurations are the 1/4 degree and at 75 vertical levels and cover the period 1993–2020. The GLORYS2V4-FREE is forced by the ERA-Interim atmospheric field. As for the biogeochemical model, the PISCES model has 24 prognostic variables and simulates biogeochemical cycles of oxygen, carbon, and the main nutrients controlling phytoplankton growth (nitrate, ammonium, phosphate, silicic acid, and iron) (Coralie et al. 2019). All of the anomaly fields in this study are relative to the climatological monthly mean during 1998–2020.

2.2 Method

2.2.1 ENSO, NPMM, and NTPO indices

The ENSO index is defined as the normalized SST anomalies averaged over the Niño 3.4 region (5° S–5° N and 170° W–120° W). The NPMM index is defined as the normalized SST anomalies averaged over the subtropical northeastern Pacific (15°–25° N and 150°–120° W) after subtracting the anomalies regressed on the Niño 3.4 index (representing the influence of the ENSO) (Amaya 2019; Ding et al. 2022). The NTPO region of interest is defined here as 5°–20° N and

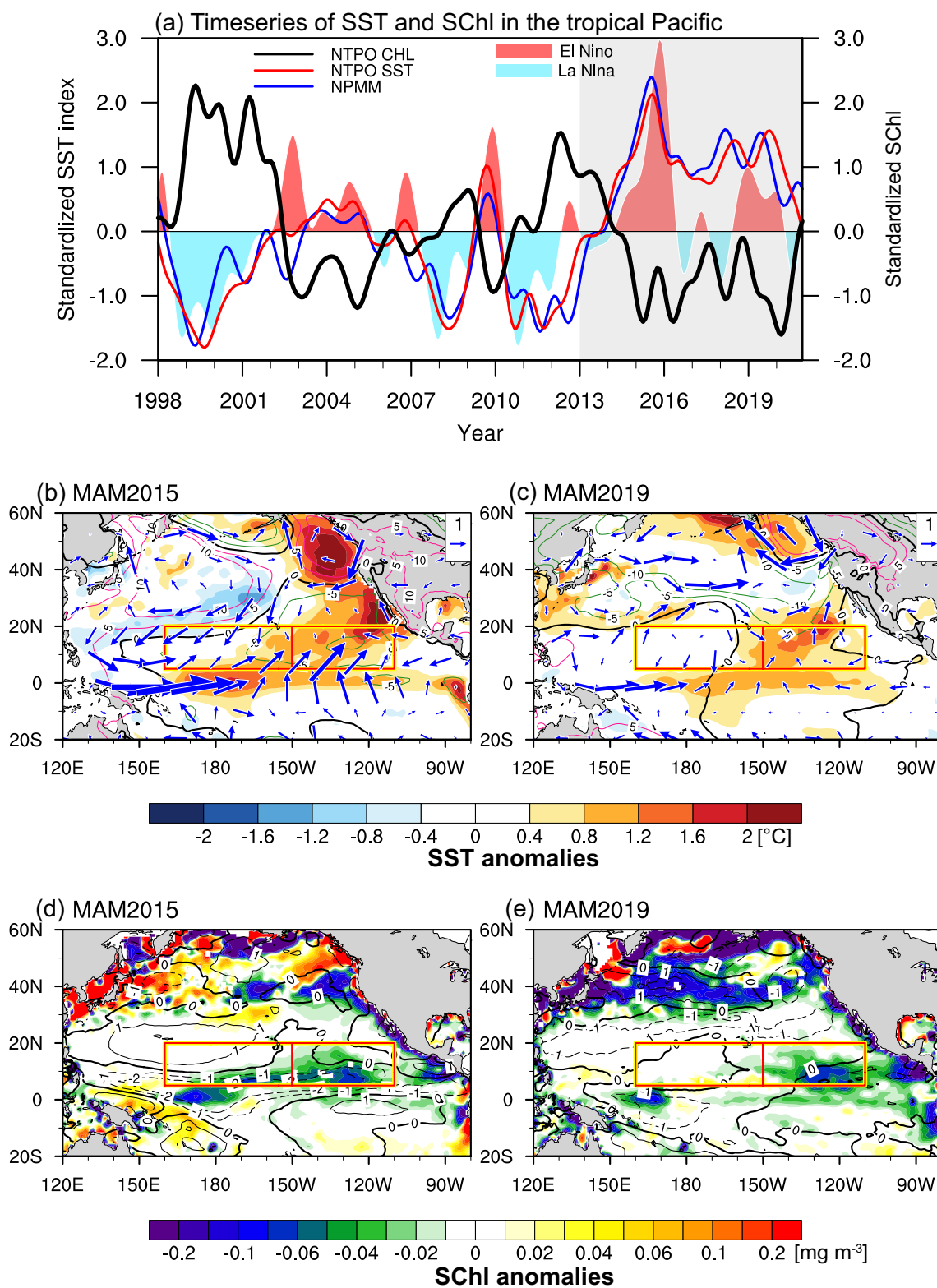


Fig. 2 **a** Time series of standardized Niño3.4 index (El Niño/La Niña conditions are shown by blue/pink shading), CHL (black curve) and SST (red curve) anomalies in the NTPO, and NPMM index (blue curve). The time series is low-pass filtered with a cutoff period of 2 years. Gray shading denotes the persistent warm period in NTPO (2013–2020). **b, c** Interannual SST (shaded), SLP (contour), and wind

field (vector) anomalies during March–April–May (MAM) 2015 and 2019, respectively. **d, e** are the same as **b, c** but for SChI (shaded) and wind speed (contour), respectively. The SST data are from the NOAA ERSSTv5; SChI data are from the GlobColor project; Surface wind and SLP are from ECMWF ERA5 reanalysis data

160° E–110° W; the western (eastern) sector of the NTPO is defined as 160° E (150° W) to 150° W (110° W), named by WNTPO (ENTPO); the NTPO SST and SChI index are defined the same as the NPMM index, respectively.

2.2.2 Decomposition contributions of density change by temperature and salinity

To examine the potential effects of upper ocean density variability on the SChI concentration, we compute the squared buoyancy frequency as stratification: $N^2 = -\frac{g}{\rho} \frac{\partial \rho}{\partial z}$, where ρ and g denote seawater density and gravity acceleration, respectively. N represents the Brunt–Väisälä frequency. MLD and isothermal layer depth (ILD) are calculated as the depth where the density is higher than that at the 10 m depth by $\Delta\rho$ (ΔT), here $\Delta\rho = -\left(\frac{\partial \rho}{\partial T}\right)\Delta T$, $\Delta T = 0.2^\circ\text{C}$. Correspondingly, barrier layer thickness denotes the difference between MLD and the isothermal layer depth (ILD).

We also adopt a decomposition method to analyze the potential temperature and salinity's contributions to various fields (Zheng and Zhang 2012; Zhi et al. 2019; Zhang et al. 2022). For example, the individual contributions from potential temperature or salinity to density are calculated as follows:

$$\rho_{temp-inter} = \rho(Temp_{inter}, Sali_{inter}) - \rho(Temp_{clim}, Sali_{inter}) \quad (1)$$

$$\rho_{salt-inter} = \rho(Temp_{inter}, Sali_{inter}) - \rho(Temp_{inter}, Sali_{clim}) \quad (2)$$

where $Temp_{inter}$ and $Sali_{inter}$ represent interannually varying potential temperature and salinity fields, respectively; $Temp_{clim}$ and $Sali_{clim}$ represent climatological potential temperature and salinity fields during 1998–2020, respectively. For example, $\rho_{temp-inter}$ ($\rho_{salt-inter}$) is meant to represent the contributions of interannual temperature (salinity) anomalies to the density variability.

2.2.3 Mixed layer heat budget

Following Cronin et al. (2015), the mixed layer heat budget can be calculated as follows using GODAS output:

$$h \frac{\partial T}{\partial t} = \frac{Q_0 - Q_{pen}|_{z=-h}}{\rho_0 C_p} - hu \cdot \nabla T - \left(W_{-h} + \frac{dh}{dt}\right)(T - T_{-h}) + \left(k \frac{\partial T}{\partial z}\right)_{z=-h}; \quad (3)$$

where h denotes the MLD, T and u are the vertical mean temperature and horizontal velocity within the ML; Q_0 is the net surface heat flux into the ocean, and Q_{pen} is the solar radiation penetrated out of the bottom of ML according to shortwave penetration scheme (Murtugudde et al. 2002);

W_{-h} (T_{-h}) is the vertical velocity (temperature) at the base of the mixed layer; k is vertical diffusion coefficient; the third and fourth terms on the right-hand side of Eq. 3 denote the entrainment-detrainment and vertical diffusion at the ML base, which is treated as residuals.

2.2.4 Ocean General Circulation Model (OGCM) experiments

We employ the Regional Ocean Modeling System (ROMS) to examine the related dynamical mechanism responsible for this persistent warming event. The ROMS is a free-surface, hydrostatic ocean model solving the primitive equations on topography-following coordinates (Shchepetkin and McWilliams 2005). The model domain covers the entire tropical Pacific and North Pacific (40° S–65° N, 110° E–70° W), with the horizontal resolution being $1/3^\circ \times 1/3^\circ$ to sufficiently resolve the current structure in the equatorial region and 50 s -coordinate levels in the vertical direction. The model is initialized by the WOA09 fields and then spin-up 30 years of forced NCEP/NCAR climatological fields (i.e., wind stress, net heat flux, and freshwater flux). Then, the 6-h atmospheric forcing data for NCEP/NCAR used in this study are adopted to calculate the flux field through the flux bulk formula.

The model is integrated from 1979 to 2022 with a 6-day output for analysis (i.e., control experiment). In the sensitivity experiments, the wind field is prescribed as its climatological field during 1979–2022 to represent the impacts of heat flux and freshwater flux on the Pacific (Wind-clim). The differences between the control and sensitivity experiments represent the wind impacts. Because precipitation effects on the ocean dynamics at the interannual timescale are relatively weak (figure not shown), the interannual signals in the Wind-clim can be attributed to the variation due to heat flux forcing (i.e., humidity, air temperature) under the climatological wind speed.

3 Observed physical-biogeochemical characteristics in the NTPO

3.1 Persistent warming in the NTPO

During 2013–2020, prominent warm SST anomalies were observed in the NTPO (Fig. 1a), which were tightly linked to the two remarkable MHW or Blob events (Amaya et al. 2020). The two Blob events exhibited the observed most significant SST anomalies emerging in March 2015 and March 2019, respectively. These extreme events further led to a warming trend in the NTPO (Fig. 1c) associated with an observed decreasing SChI trend from 1998 to 2020 (Fig. 1b). Therefore, the persistent warming during 2013–2020 in the

NTPO significantly affected the recent trend in the marine physical environment and ecosystem.

The persistent warming in the NTPO tended to be maintained by the ENSO and the northern Pacific atmospheric circulation anomalies. This persistent warming can be seen to originate from the 2014–2015 North Pacific marine heat-wave, which gradually developed from the Gulf of Alaska to the Pacific coastal boundary of North America. Then, it emerged in the NTPO (Fig. 2b), leading to record-high SST anomalies during the boreal spring of 2015 (Fig. 2a). The warm SST anomalies along the Baja California can excite anomalous cyclonic circulation in association with low sea level pressure (SLP) center in the eastern sector of the NTPO; thus, the anomalous westerly winds superimposed on the background trade winds, reducing the wind speed and upward latent flux, subsequently warming the underlying ocean (Fig. 2b). A similar condition occurred in March 2019 but with a relatively weaker amplitude in SST (Fig. 2c). With the southwestward development of warm SST anomalies, an El Niño-like structure formed during boreal summer and fall in 2015 and 2019; the equatorial westerly winds were seen to develop through a positive Bjerknes feedback through warm SST, weakened easterly trade winds, and a deepening thermocline (Figs. 2a and S1). Additionally, remote SST forcing from the central equatorial Pacific excited atmospheric teleconnections in the extratropics that reenergized the northern Pacific atmospheric variability (e.g., NPO) and sustained the persistent warming (Ding et al. 2022). Thus, the two persistent El Niño events (2014–2016 and 2018–2020) happened in succession (Figs. 2a, S2, and S3).

3.2 Consecutively low SChI in the NTPO

The consecutive low SChI anomalies emerged in the selected period (2013–2020), which was closely related to persistent warming and low surface wind speed. The extremely low anomalies in SChI exceeding one standard deviation occurred in 2015, 2016, 2018, 2019, and 2020 (Figs. 2a and 3). The correlation between SChI and SST anomalies attained -0.68 at the 99% significance level, indicating that the responses of SChI in the NTPO was closely related to the surface temperature condition. During the boreal spring of 2015, for example, anomalous SChI emerged in the entire NTPO, with a maximum value ($< -0.05 \text{ mg m}^{-3}$) being in the eastern sector of NTPO (Fig. 2d), in association with the spatial pattern of low wind speed. In contrast, during the boreal spring of 2019, anomalous SChI only concentrated in the ENTPO, accompanied by local SST warm anomalies but with relatively weak change in wind speed (Fig. 2e). The SST anomalies in the NTPO further facilitated the development of El Niño during wintertime, and subsequently led to negative SChI anomalies in the NTPO by anomalously eastward current (Figures S1 and S3), similar to other El

Niño events reported by Radenac et al. (2012). Furthermore, two consecutive El Niño sustained the negative anomalies in SChI during 2013–2020. The net primary production also exhibited a persistent decline during this warming period, reflecting consistent ecosystem responses in the NTPO (Figure S4).

4 Dynamical processes responsible for SST and SChI anomalies

4.1 An overview of oceanic process changes in the NTPO

The oceanic processes responsible for the persistent warming and low SChI were distinct in the western (WNTPO) and eastern (ENTPO) sectors of the NTPO. The increase in density stratification was the dominant factor that led to persistent warming and low SChI in the WNTPO, while downwelling played a crucial role in controlling these anomalies in the ENTPO. In particular, the persistent warming mainly emerged in 150°E – 100°W in association with low SChI that was mainly located between 180° and 100°W (Fig. 3). Still, sea level anomalies (SLA) exhibited out-of-phase evolution in the ENTPO and WNTPO near 150°W during 2015–2016 and 2019–2020 (Fig. 3c). In the ENTPO, the persistent positive SLA anomalies can be seen, which corresponded to a suppression of the thermocline. In contrast, in the equatorial ocean, El Niño and La Niña events appeared alternately (Fig. 3d–f).

In the WNTPO (west of 150°W), the vertical structure of density anomalies exhibited opposite changes in the mixed layer and upper limb of the thermocline from EN4 data (Fig. 4b), indicating that the enhanced stratification acted to dominate the decline in SChI. For example, an increase in sea surface temperature (SST) firstly induced anomalous westerlies in the western sector of the NTPO, which acted to reduce wind speed and subsequently enhanced upper ocean stratification (Fig. 4a, d), consequently leading to a decrease in surface nitrate (a dominantly limit factor to the nutrient) and SChI. Meanwhile, the positive wind stress curl in the subsurface layer induced a positive Ekman pumping and subsurface cooling (Fig. 2c, d, 4b). As shown in Fig. 4d, the stabilized vertical structure (Fig. 4d) overwhelmed the upwelling due to Ekman pumping, and consequently led to a slight decrease in SChI, especially in 2015, 2019, and 2020, which was mainly attributed to the surface warming and freshening (Fig. 4a–c).

In the ENTPO (east of 150°W), suppression of the thermocline/nutricline due to negative wind stress curl led to a reduction in nutrients and subsequent decreased SChI (Fig. 3b). The anomalous easterlies due to the positive phase of NPMM induced an anomalous anticyclone (Fig. 2c) and subsequently

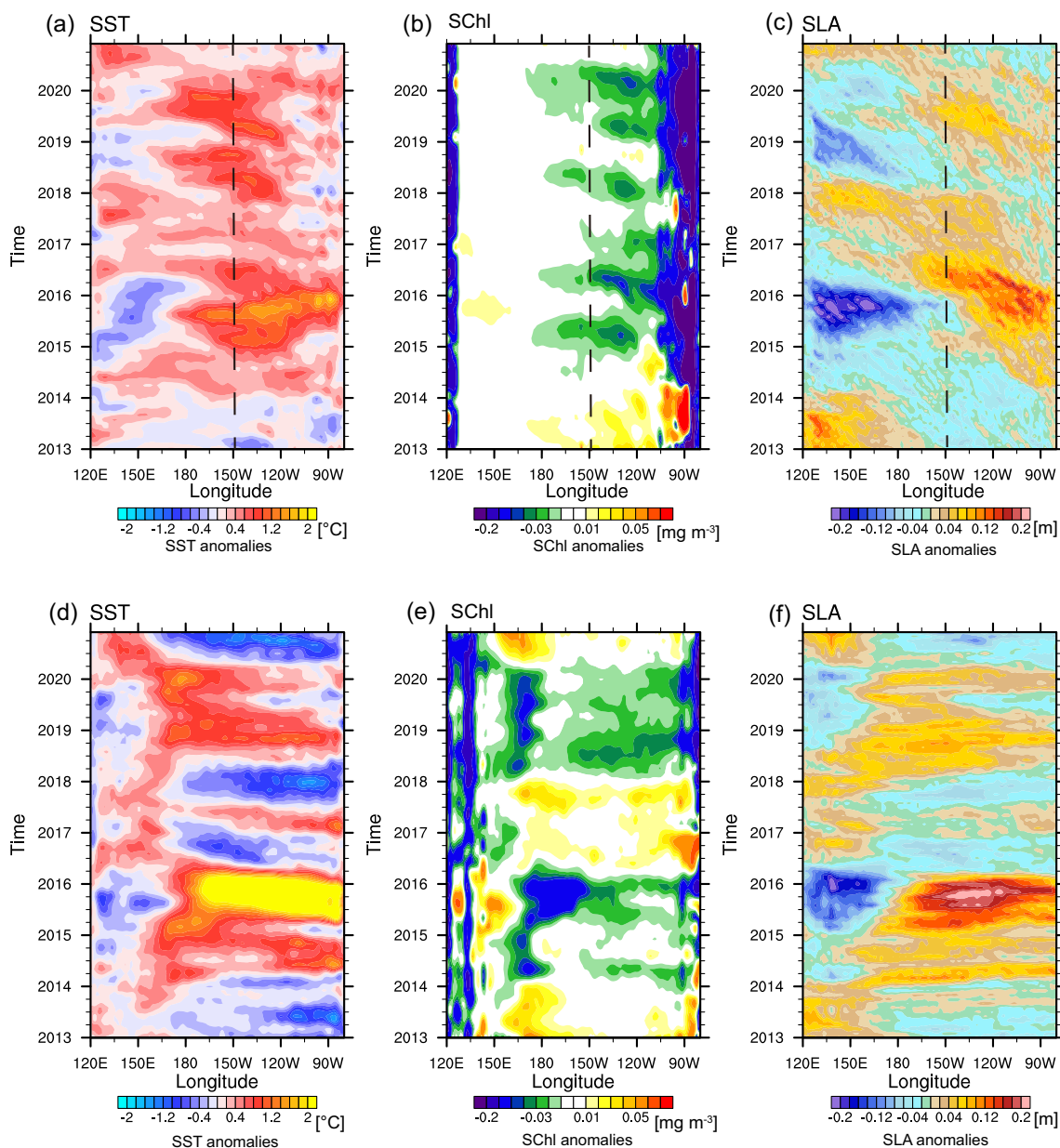


Fig. 3 Longitude-time Hovmöller diagrams for equatorial anomalies in SST (a, d), SChl (b, e), and SLA (c, f) for the period of 2013–2020. The upper (lower) panel displays the meridional average in

corresponding variables over 2° S–2° N (5° N–20° N). SST fields are from the NOAA ERSSTv5; SChl fields are from the GlobColor project, SLA fields are from the CMEMS altimeter satellite gridded data

led to positive SLA signals propagating westward as Rossby waves (Fig. 3c). The downwelling processes can be seen in the time-depth evolution of temperature-salinity in Fig. 5b, c; the subsurface warming (freshening) further propagated downward, accompanying the depressing of the thermocline starting from spring in 2015 and 2018, respectively (Fig. 5b). In addition, the contribution of temperature to the density was more dominant in the subsurface layer (Fig. 5e). In contrast,

the contribution from salinity to the mixed layer was comparable with that from temperature (Fig. 5c–f). Synchronous correlation analysis also revealed the barrier layer change was not remarkable (Figure S5). Given the prominent role of surface warming in the NTPO environment, the related mechanisms were further investigated using heat budget analysis and numerical experiments as follows.

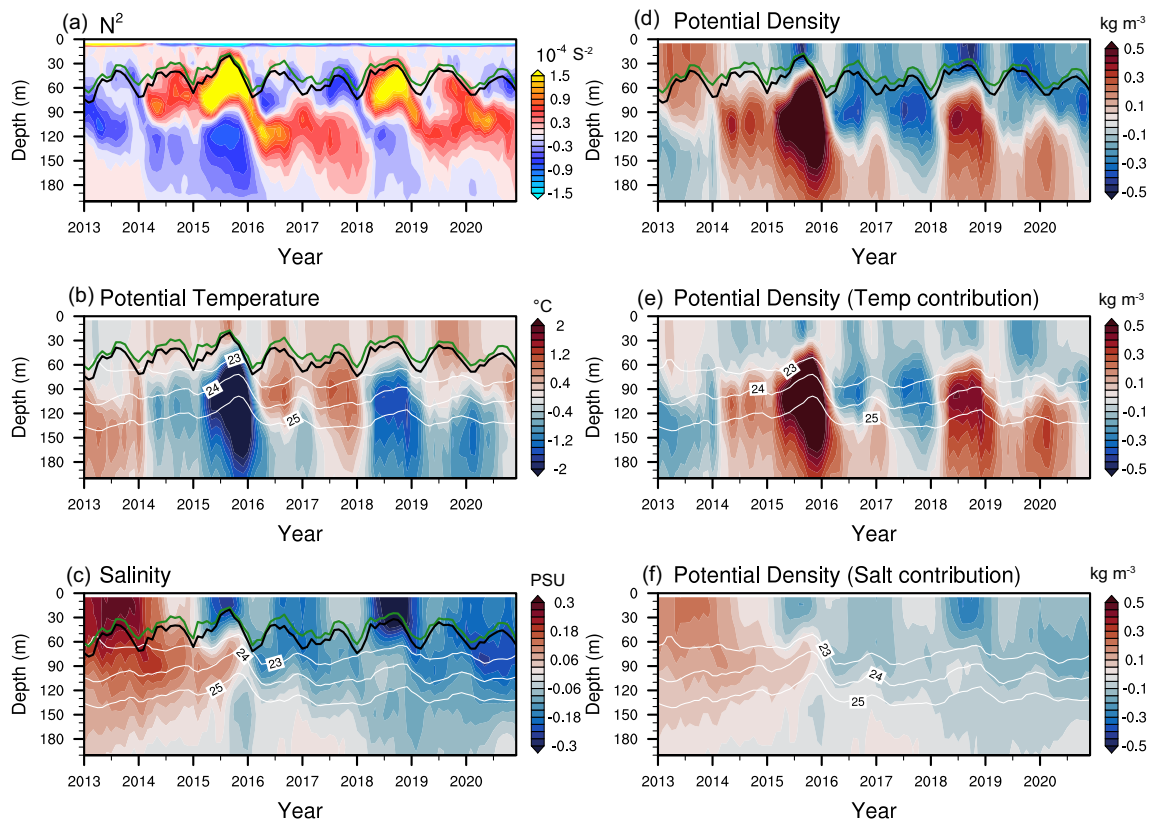


Fig. 4 Time-depth (0–200 m) section for density-related variable anomalies averaged over the WNTPO (5° N– 20° N, 160° E– 150° W) from January 2013 through December 2020; **a** squared buoyancy frequency (N^2), **b** potential temperature, **c** salinity, **d** potential density, **e** potential density change due to temperature variation, **f** poten-

tial density change due to salinity variation. Green (black) contours in **a–d** represent the depths of the barrier layer and mixed layer, and white lines in **b–f** show 23, 24, and 25 kg m^{-3} isopycnal surfaces. The potential temperature and salinity data are from the EN4 at Met Office Hadley Centre observations datasets

4.2 Mixed layer heat budget analysis

The mixed layer heat budget analysis derived from GODAS reanalysis revealed that the net surface heat flux acted to dominate the NTPO persistent warming in 2014–2016, but the vertical mixing and entrainment efficiently affected the SST warming in 2018–2020, especially in the WNTPO (Fig. 6a). In contrast, the contribution from the horizontal advection was relatively weak.

During the 2014–2016 warming (pink shading in Fig. 6), an increase in net surface heat flux tended to maintain the positive SST anomalies in the NTPO. The positive SST anomalies emerged in the spring of 2014 over the NTPO and peaked in the fall of 2015 by 1.5°C in the ENTPO, where the net surface heat flux reached $0.6^{\circ}\text{C}/\text{month}$, which can be compensated for by the enhanced cooling due to vertical mixing and entrainment, and the cooling effect was more prominent in the WNTPO. In contrast, the horizontal advection was relatively weak in the period.

During 2018–2020 (blue shading in Fig. 6), the net surface heat flux exhibited a net cooling impact on the

SST in the WNTPO, while the weakened vertical mixing and entrainment dominated the surface warming. The subsurface warming exceeded the mixed layer warming in the WNTPO (Figs. 4, 5); subsequently, the enhanced Ekman pumping velocity can transport warmer water into the mixed layer and led to SST warming. In contrast, the enhanced Ekman suction (downwelling processes) sustained the weakened vertical mixing in the ENTPO. This distinct response in the vertical temperature structure further confirmed the previous hypothesis, i.e., the NPMM-induced anomalous cyclonic (anti-cyclonic) circulation over the WNTPO (ENTPO) led to the consistent warming in the NTPO.

Different from the dominant role of net surface heat flux on the SST in the NTPO, the surface warming in the equatorial ocean was mainly attributed to dynamical process changes (Fig. 6b); i.e., the horizontal advection (vertical mixing and advection) was dominant in the Niño4 (Niño3) region during 2013–2020, respectively.

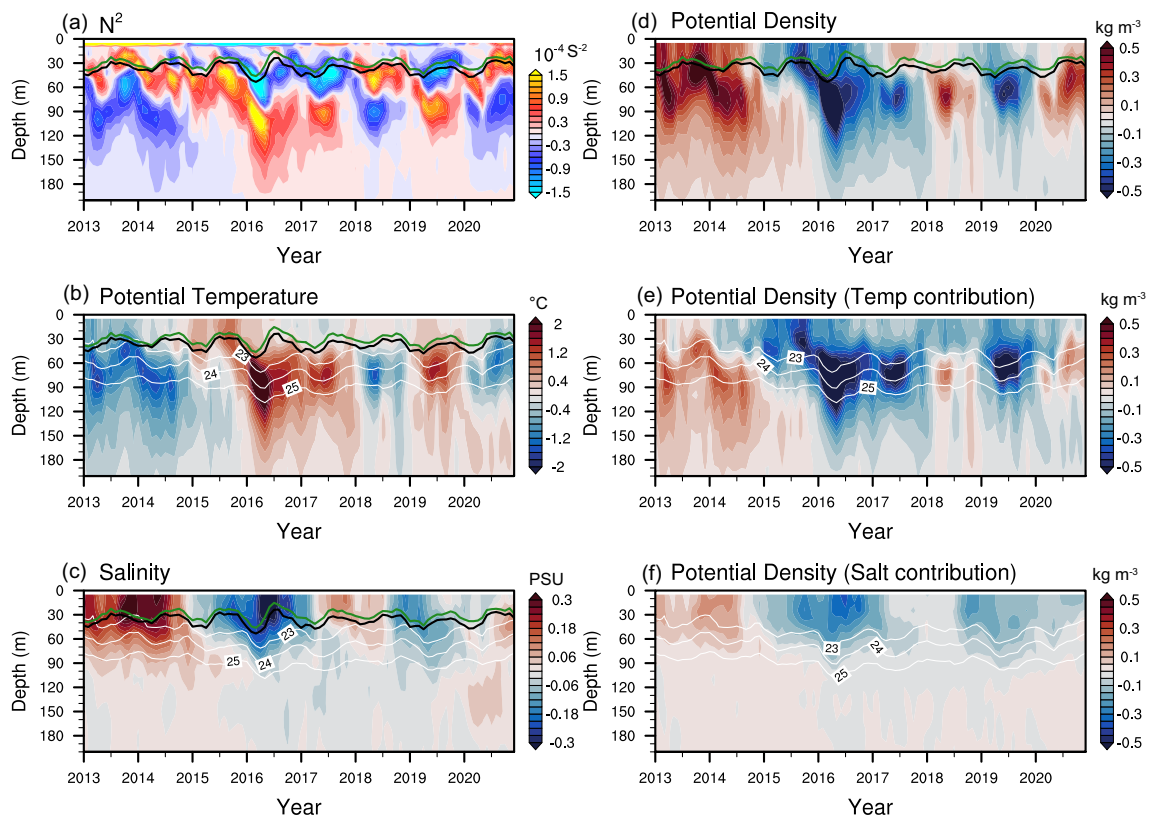


Fig. 5 The same as in Fig. 6 but for in the ENTPO (5° N–20° N, 150° W–110° W)

4.3 OGCM simulations

Given the key role of surface wind and heat flux in determining surface warming in the NTPO, we performed two sets of experiments to isolate the impacts of surface wind and heat flux on the SST anomalies. Model results demonstrated that the decreased latent heat flux due to weakened surface wind dominated the surface warming during 2013–2020. Under the forcing from the NCEP/NCAR atmospheric field, the ROMS can reasonably well simulate the SST anomalies in the NTPO during two peak periods (boreal spring of 2015 and 2019).

During March–April–May (MAM) 2015, the positive SST anomalies extended from the northwestern coast of North America to the central equatorial Pacific; the ROMS can reasonably simulate the coastal warming but overestimated the central Pacific warming (Fig. 7a, b). When the wind field was fixed as the climatological field, the surface warming in the northeastern coast of the Pacific was slightly weakened, indicating that the surface heat flux related to atmospheric humidity and air temperature tended to dominate the SST warming (Fig. 7c), which was also reported in a recent study by Chen et al. (2023). In the NTPO, the SST warming tended to be determined by the combined effect of wind and heat flux; quantitatively, the wind anomalies

contributed to SST variation by 35%, while other atmospheric forcings (e.g., humidity) contributed about 65%. On the contrary, in the equatorial Pacific, the wind anomalies dominated the SST change, contributing to 68% variation during MAM 2015.

Another warming peak occurred in MAM 2019 when SST anomalies exhibited a typical NPM pattern (Fig. 8a, b). The ROMS can reasonably simulate the distribution of SST, with two cores of positive SST anomalies being reproduced (Fig. 8b). When the wind effect was removed, the warm SST anomalies were still retained in the ENTPO (Fig. 8c), indicating that the atmospheric humidity and air temperature played a predominant role. On the contrary, a slight cooling was seen in the WNTPO, which can be attributed to the combined effects of wind and heat flux (Fig. 8c, d), similar to the results from heat budget analysis.

4.4 Biogeochemical responses to the dynamical change: a hindcast simulation

Persistent warming in the NTPO was closely related to unusual biogeochemical responses by affecting the redistribution of nutrients and temperature-light conditions. The NTPO is located between the subtropical gyre and equatorial Pacific, where the iron and nitrate can jointly limit

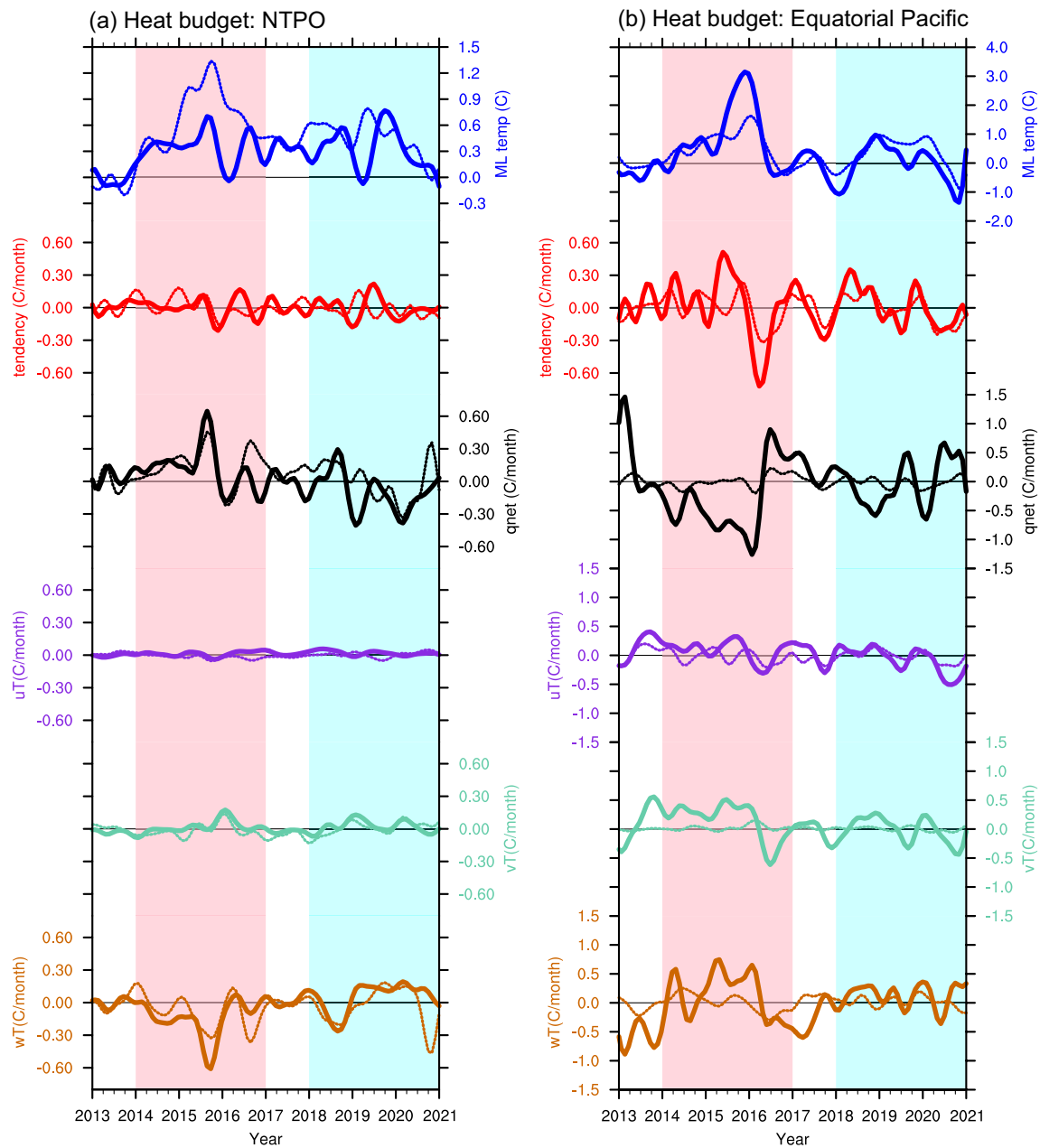


Fig. 6 Mixed layer heat budget estimated in GODAS reanalysis in the NTPO **(a)** and the equatorial ocean **(b)** during 2013–2020. The solid (dash) line denotes the estimation in the WNTPO (ENTPO) in **a** and Niño3 (Niño4) regions. Budget terms include tendency term (blue

lines), total surface heat flux (red lines), zonal advection (yellow lines), meridional advection (green lines), and entrainment/residual (purple lines)

the phytoplankton growth (Arteaga et al. 2014; Nakamura and Oka 2019; Browning and Moore 2023; Browning et al. 2023). Therefore, the responses of subsurface nutrients to persistent warming were further investigated in detail.

The related biogeochemical response was analyzed using a hindcast biogeochemical modeling output from CMEMS. The CMEMS model well captured the evolution of SchI in the NTPO and equatorial Pacific; the persistent decreasing SchI in the NTPO was comparable with the satellite

observation (Fig. 9a); in the equatorial Pacific, the fluctuations in SchI in association with ENSO were also well reproduced (Fig. 9b). The vertical structure of nutrients further demonstrated that the enhanced stratification dominated the reduction in the WNTPO, but the negative wind stress curl-induced downwelling acted to reduce the nutrient supply within the mixed layer. The correlation map revealed that the anomalies in SchI were highly dependent on the nitrate in the NTPO, while the contribution from iron was

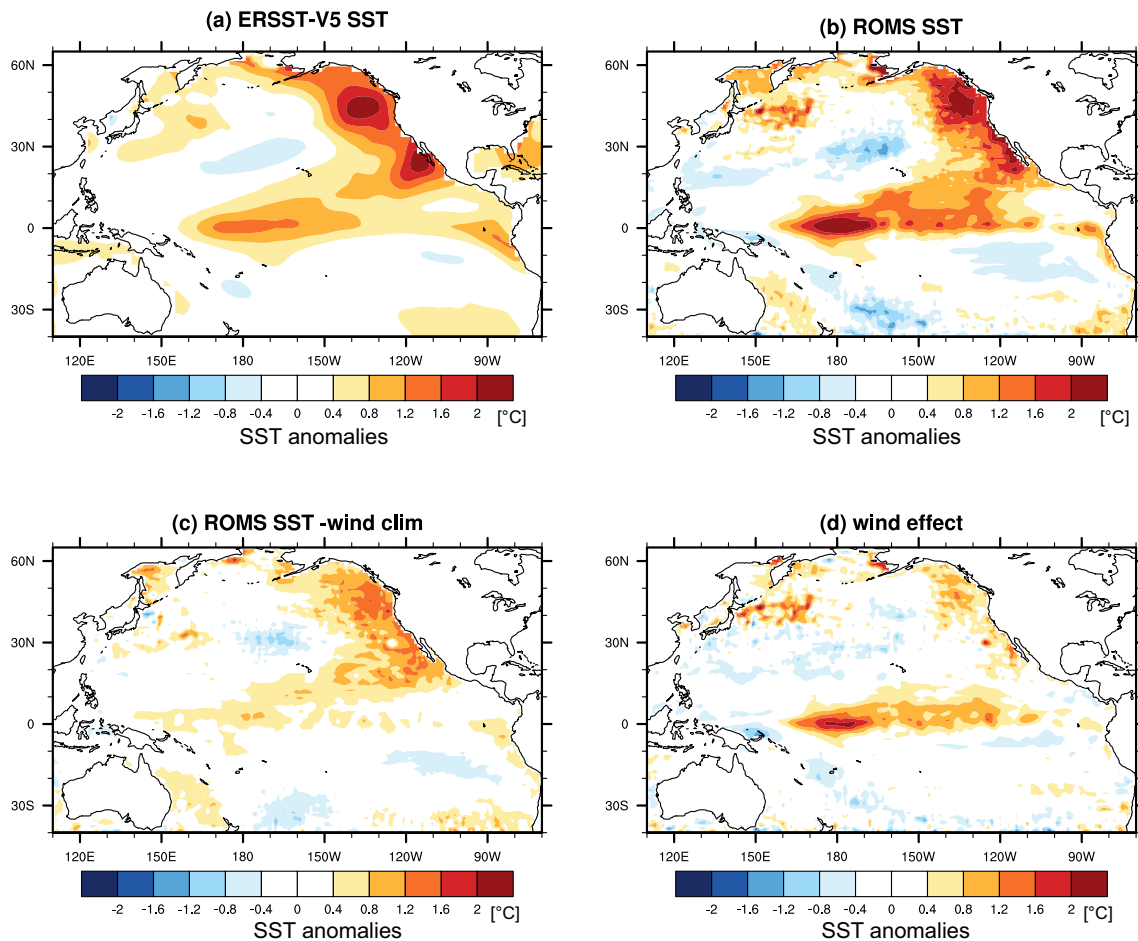
MAM 2015


Fig. 7 SST anomalies during March–April–May (MAM) 2015 from ERSST-V5 (a); CTRL simulation (b); Wind-clim simulation (c); the inter-annual wind effect (d); **b–d** are from ROMS simulations forced by the NCEP/NCAR atmospheric fields

negative (Fig. 10). A recent observational study suggested that nitrate was so low that the supply of nitrogen stimulated small phytoplankton increases in the NTPO (Browning and Moore 2023; Browning et al. 2023). Meanwhile, more in-situ experiments suggested that the combined supply from nitrogen and iron can further boost phytoplankton pigment biomass accumulation in comparison to nitrogen alone (Browning and Moore 2023; Browning et al. 2023). Therefore, the CMEMS model can partially reproduce the limited condition of nutrients. In contrast, the correlation between SchI and iron was highly positive in the eastern tropical Pacific (Fig. 10b), where the phytoplankton growth was iron-limited. In addition, silicon and phosphorus also contributed to the SchI variability in the equatorial ocean (Fig. 10c, d).

In the WNTPO, the vertical structure of nutrient anomalies exhibited a consistent “two-layer” distribution, with a negative anomaly in the upper mixed layer and a positive anomaly in the subsurface layer (Fig. 11b–d). The upper

positive anomaly in nitrate (or phosphorus) can be attributed to the enhanced density stratification (Fig. 4), which suppressed the subsurface nitrate-rich water transported into the mixed layer. Due to the positive Ekman pumping, a positive nitrate anomaly was clearly found in the subsurface layer (Fig. 11b). This vertical structure further supported the previous hypothesis that the NPM-induced cyclonic circulation contributed to the physical and biogeochemical changes in the WNTPO (Fig. 11b).

In the ENTPO, vertically consistent negative anomalies in nitrate were clearly seen during 2014–2016 (Fig. 11f) and relatively weak during 2019–2020, highlighting the key role of downwelling processes in redistributing the nutrients. The persistent negative anomalies emerged in the upper 200 m associated with negative Ekman pumping velocity, similar to the upper-temperature structure (Fig. 11e). This unified vertical structure can also be seen during 2019–2020, albeit with relatively weak anomalies. The biogeochemical response to this persistent warming effect indicated that the

MAM 2019

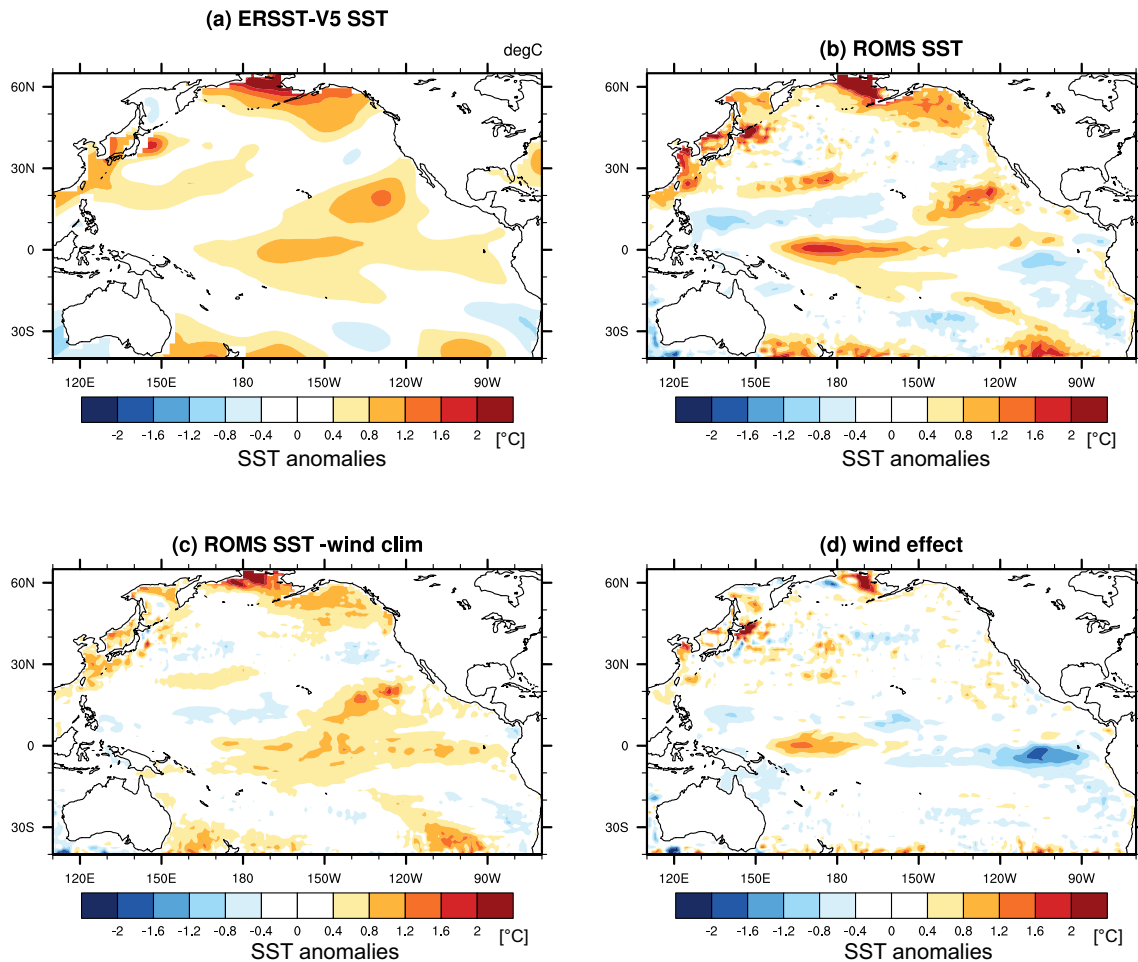


Fig. 8 SST anomalies during March–April–May (MAM) 2019 from ERSST-V5 (a); CTRL simulation (b); Wind-clim simulation (c); the inter-annual wind effect (d)

dynamical processes were different in the western and eastern sectors of the NTPO, which was highly dependent on the atmospheric circulation induced by the climate modes.

5 The roles of climate modes in the persistent warming

To understand the role of climate modes in driving the NTPO persistent warming, we adopted a singular value decomposition (SVD) analysis in the tropical and northern Pacific for SCHl and SST based on the observational data (Fig. 12). The results suggested that the NPMM acted to dominate the persistent warming and low-SCHl in the NTPO, while ENSO played a secondary role. The spatial pattern of the first mode in SVD showed the typical El Niño-like pattern, with the positive SST anomalies located in the tropical and subtropical oceans, which further extended into

the subpolar region along the coast of Northern America (Fig. 12a). Meanwhile, negative SCHl anomalies emerged in the equatorial Pacific and extended to the subtropical Pacific (Fig. 12b). The principle components (PC) in the 1st mode (PC1) exhibited a tight correlation with the Niño3.4 index, indicating the 1st mode was dominated by the ENSO events, which explained the variation of 65.7% in the Pacific (Fig. 12c). The second mode in SVD exhibited an NPGO or NPMM-like pattern with positive anomalies in the subtropical oceans and negative SST anomalies in the eastern tropical Pacific (Fig. 12d). SCHl showed a unified decrease in the NTPO (Fig. 12e), similar to the recent persistent SCHl anomalies (Fig. 2). The PC2 in SST exhibited a tight correlation with the NPMM index but a relatively weak relationship with ENSO (Fig. 12f). Therefore, the similar pattern with recent persistent warming suggested that the NPMM controls current unusual events. The third mode exhibited an El Niño rebound condition (Fig. 12g), with surface

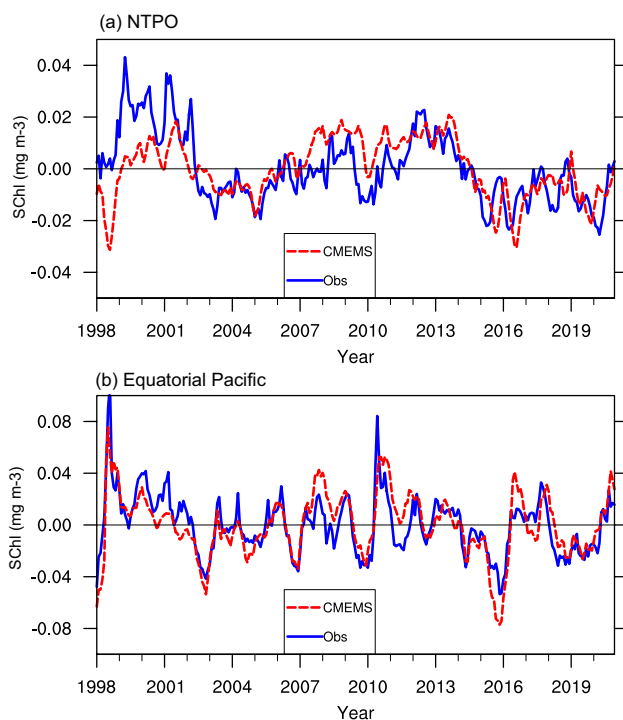


Fig. 9 Validation for SChl from the CMEMS-model (red lines) with observation (black lines) during 1998–2020 in the NTPO (a) and the equatorial ocean region (b)

cooling emerging in the equatorial Pacific, accompanied by an increase in SChl as suggested by previous studies (Park et al. 2011; Lim et al. 2022).

Similar results were found using the regression method to emphasize the contribution of NPMM and ENSO to persistent warming in the NTPO (Fig. 13). Figure 13a showed that SST anomalies during MAM were firstly regressed on the NPMM index during JFM with retaining the ENSO effect, corresponding to the regression map of SChl on the NPMM index shown in Fig. 13b. This case indicated that the combined impact of ENSO and NPMM on the NTPO was remarkable and coincides with the recent surface warming and low chlorophyll condition. After removing the ENSO effect by subtracting the Niño3.4 index during D(0)JF in the original SST and SChl, the sole NPMM effect was shown in Fig. 13c, d. The impacts of NPMM were more concentrated in the off-equatorial region and subtropical Pacific; the SST anomalies in the equatorial Pacific were negligible. We further extracted the ENSO effects by making the difference between the above two conditions (Fig. 13e, f); the results suggested that during the boreal spring (MAM), the contribution of NPMM to the NTPO was relatively dominant, especially in SST. Nonetheless, the ENSO effect played an opposite role with NPMM in the SChl evolution in NTPO; quantitatively, using the simple regression method, the NPMM contribution to the variations of SChl in the

NTPO during boreal spring was 121%, while the contribution from ENSO to SChl variation in NTPO was about -21%. An El Niño event began to decay during the boreal spring, which can be first seen in the subsurface anomalies, including thermocline change and the related nutrient change. As shown in Fig. 13f, a positive anomaly in SChl emerged in the equatorial region when the SST still exhibited a positive anomaly (Lim et al. 2022a). In the off-equatorial region, the SChl also showed a negative anomaly band, indicating that the contribution of El Niño still existed, which mainly stemmed from the zonal advection as shown in Radenac et al. (2012).

The relationship between NPMM SST during JFM and NTPO SChl was examined using scatterplot during MAM from satellite observation, which indicated a tight correlation between NPMM and NTPO ($R=0.45$, $P<0.01$), especially during the persistent warming period (2013–2020); the warm SST anomalies in association with NPMM and low SChl in the NTPO were well located in the fourth quadrant. Meanwhile, the correlation between Niño3.4 SST during DJF and NTPO SChl was also positive with $R=0.45$, $P<0.05$. This close relationship was mainly attributed to the consistent response of SChl in NTPO to La Niña events. Nonetheless, the recent persistent low SChl corresponded to the warm phase of NPMM during 2015, 2017, 2018, and 2019 (Fig. 14a).

6 Discussions

6.1 Potential impacts of decreasing SChl on the ocean dynamics

Under persistent warming and decreasing SChl conditions, the chlorophyll-induced heating feedback on SST and stratification can not be negligible. Previous studies demonstrated that chlorophyll can modulate the tropical Pacific climate by affecting the vertical distribution of shortwave radiation in the upper ocean. The redistribution of shortwave radiation changes the thermal structure and related stratification, which further leads to a change in vertical mixing and ocean circulation (Murtugudde et al. 2002; Zhang et al. 2009; Gnanadesikan and Anderson 2009; Zhang et al. 2019; Tian et al. 2021a). However, the impacts of SChl changes in the NTPO on the tropical Pacific climate remain unknown. As shown in Figure S8, the spatial pattern of interannual variability of SChl exhibited a unique triple-pole structure, with a substantial variability center being in the NTPO and others being in the equatorial ocean. A series of studies found that the variability of interannual SChl anomalies in the equatorial region can modulate the ENSO variability by affecting the thermocline feedback (Tian et al. 2021b). Therefore, due to the substantial effect on the variation of

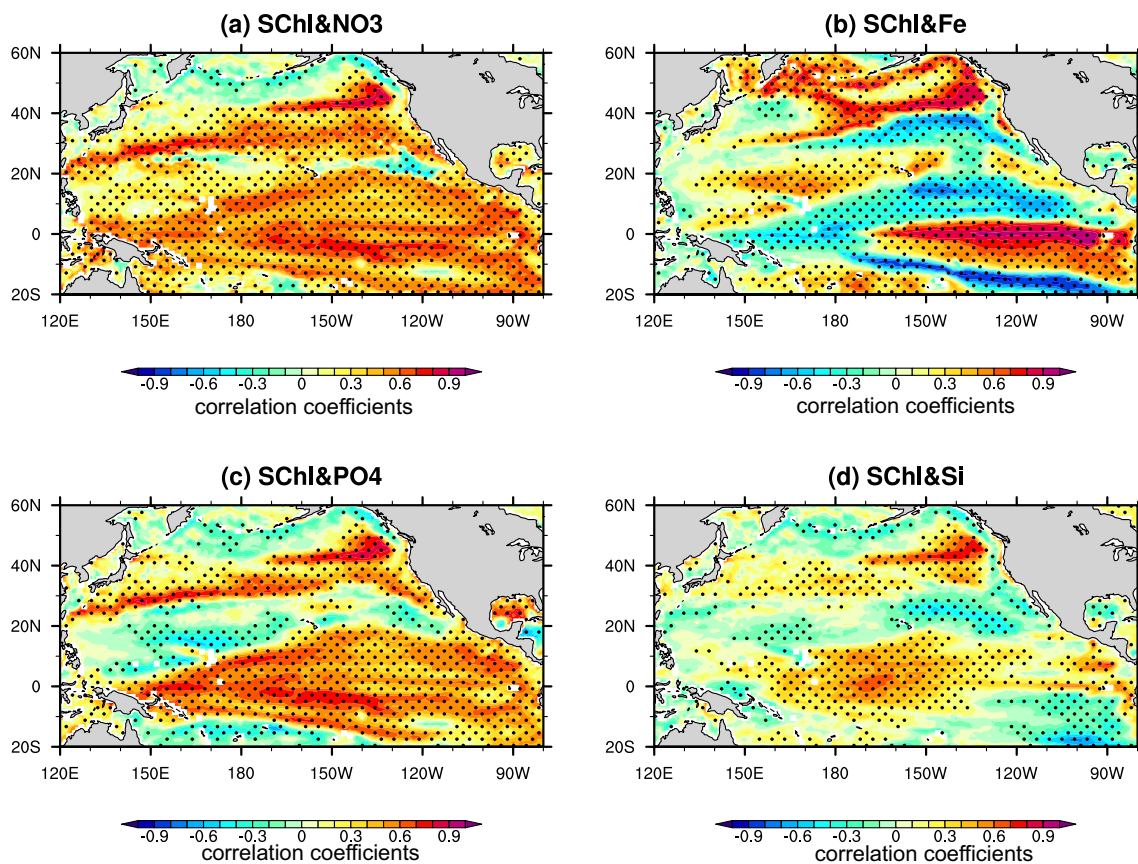


Fig. 10 Correlation map between surface chlorophyll and nutrients (nitrate in **a**, iron in **b**, silicon in **c**, and phosphorus in **d**) averaged over 0–100 m derived from the CMEMS model during 1998–2020.

penetration attributed by SChl, the variation of SChl in the NTPO can exert feedback on the local ocean dynamics and subsequently modulate the interaction between the tropics and subtropics, which should be examined in the future.

6.2 Impacts of persistent warming on the carbon cycle and acidifications

The persistent warming and low-SChl can further change the carbon cycle in the NTPO. The tropical Pacific is a carbon source relative to the global ocean carbon sink (Tian et al. 2019). Meanwhile, the NTPO is the region where a transition is seen between the subtropical ocean carbon sink and the tropical Pacific carbon source. The biogeochemical processes due to locally physical environment change can affect the carbon source or sink. A recent study revealed that compound events with surface warming and ocean acidification extreme tended to easily occur more than the independent single case (Burger et al. 2022). Further analysis found that during the persistent warming period of 2013–2020, the phytoplankton carbon from CMEMS hindcast simulation tended

to be continuously decreased (Fig. 15a) and the air-sea CO₂ flux exhibited a negative anomaly with a peak reaching 0.6 mmol m² year⁻¹, which further led to enhanced acidification in the upper 200 m through the CMEMS hindcast simulations (Fig. 15b). Thus, whether the NTPO has changed from a carbon source to a carbon sink with enhanced acidification under the global warming scenario should be investigated in the future.

Stippling indicates a region above 90% significance computed from a two-tailed t-test

6.3 Multiple climate modes and their combined effects

The combined effect of ENSO and NPMM can jointly lead to this persistent warming event. As discussed in the results section, NPMM acted to dominate the recent persistent warming and low SChl events, while the contribution from ENSO was relatively weak. This conclusion was somewhat different from previous findings, which indicated that ENSO dominated the evolution of the tropical Pacific climate and biogeochemical cycles. For example, during the decay phase of ENSO, the transition from El Niño to La Niña was relatively slow in the NTPO

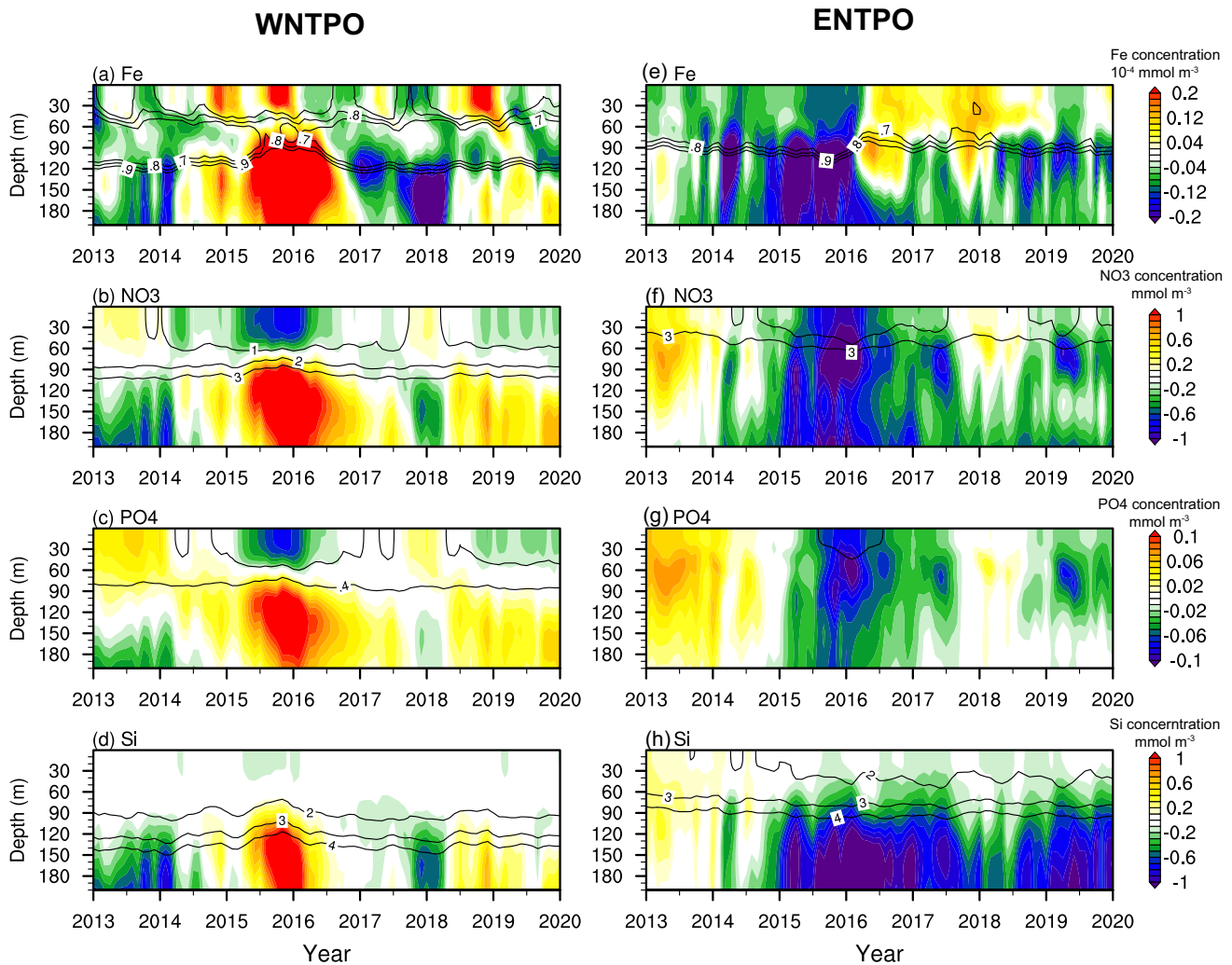


Fig. 11 Time-depth (0–200 m) section for nutrients anomalies averaged over the WNTPO and ENTPO from January 2013 through December 2020: **a, e** for Fe, **b, f** for nitrate, **c, g** for silicon, **d, h** for

phosphorous, respectively. Black contours represent the total fields. The nutrients anomalies are obtained from the CMEMS biogeochemical hindcast simulations

compared to that in the equatorial region, where the rapid ocean subsurface dynamics (e.g., Kelvin waves) terminated the warming state. In this persistent warming event, SST warming first emerged in the northeast subtropical ocean (e.g., NPMM-related region) and then gradually extended southwestward by WES feedback and peaked in the boreal spring. Therefore, NPMM dominated the SST warming during the developing phase of two ENSO events (2015–2015 and 2018–2019); subsequently, the strong or moderate El Niño sustained the persistent warming in the NTPO during its peak and decaying phase.

6.4 Potential contributions from external forcing and internal variability

Persistent warming in the NTPO can be also related to interactions between the external forcing and internal variability.

Previous studies have demonstrated that greenhouse warming can strengthen the linkage between the tropical and subtropical oceans through ocean–atmosphere interactions (Jia et al. 2021; Ding et al. 2022). However, whether the persistent warming can be attributed to anthropogenic activity remained unknown. The potential impacts of global warming on the relationship above were simply discussed using CMIP6 multi-model ensembles (Table S1). In the CMIP6 output, earth system Model (ESM) well simulated the spatial pattern of SChI response in the NTPO to the NPMM (Figures S6 and S7), and the correlation coefficient reached 0.47 with $P < 0.001$ during the historical scenario. In the SSP5-8.5 scenario, the relationship between the NTPO SChI and NPMM was slightly weakened to 0.37 but still exceeded the $P < 0.001$ significance level (Figure S9). On the contrary, the correlation between ENSO and SChI in NTPO was relatively

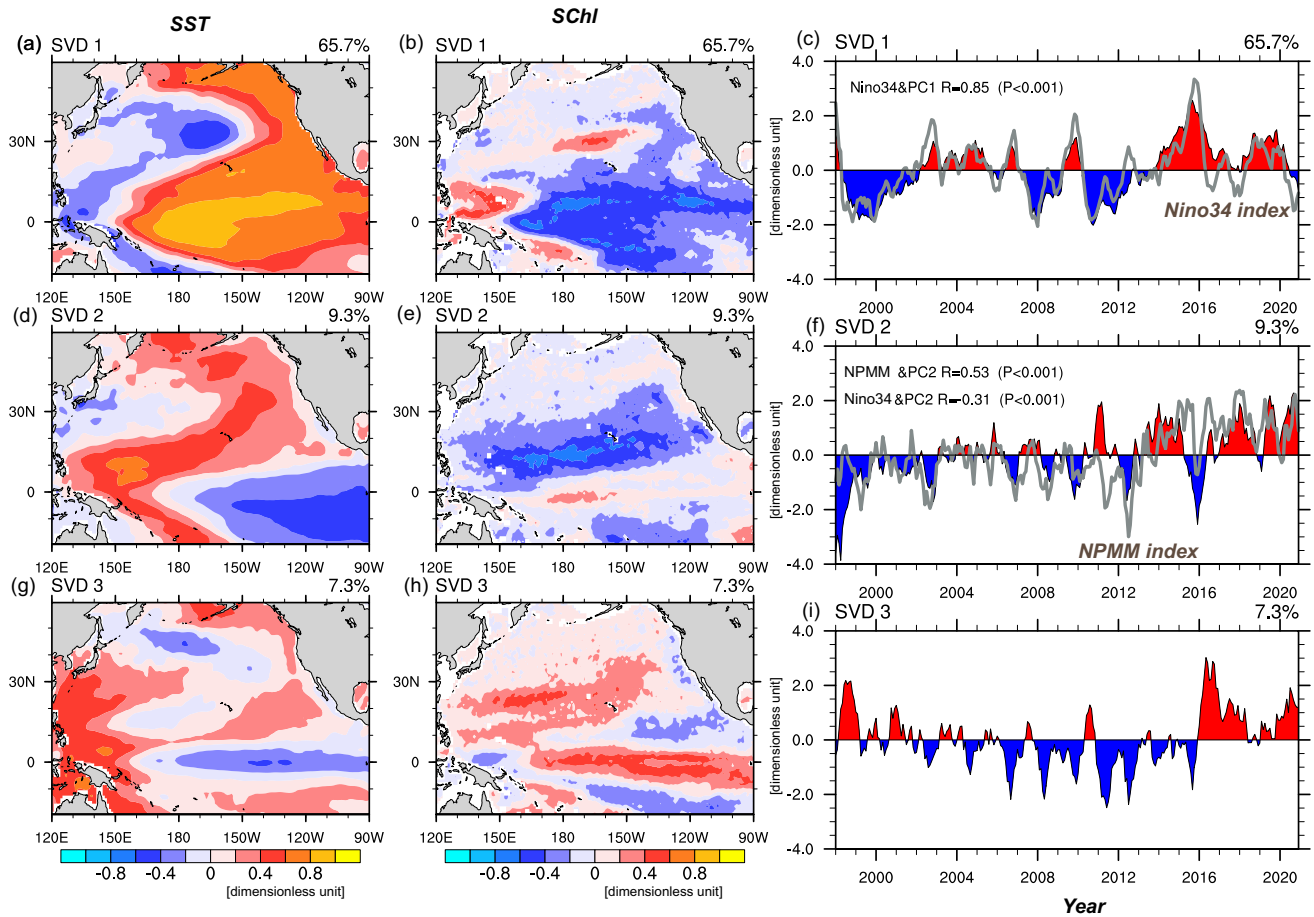


Fig. 12 Homogeneous regression map (shaded) against the first singular value decomposition (SVD1) mode between SST (a) and SchI (b). c, d and e, f are the same as a, b, but for the SVD2 and SVD3 modes, respectively; g–i the associated first three principal com-

ponent time series for 1998–2020. Gray lines in g, h represent the Niño3.4 and NPMM indexes, respectively. The SST and SchI used for SVD analysis are based on the observational data from NOAA ERSSTv5 and GlobColor Project, respectively

weak during historical scenarios ($R=0.09$, $P<0.001$). During the global warming scenario, the response of SchI in the NTPO to ENSO was insignificant, with $R=0.03$ ($P=0.316$) (Figure S9). Therefore, under the global warming scenario, the impact of NPMM on the NTPO SchI was more dominant compared with ENSO. A recent study also demonstrated that the impacts of NPMM on the ENSO were strengthened under global warming, which can be attributed to the background warming in the northern Pacific (Jia et al. 2021). Therefore, the impacts of the North Pacific on the tropical ecosystem should be investigated in the future.

In addition, the impact of decade change of the Pacific climate on this persistent warming cannot be ignored. Persistent warming (e.g., 2013–2020) might occasionally occur during the transition between the negative phase of the interdecadal

Pacific Oscillation to its positive phase (Hu and Fedorov 2017); this transition from cooling condition to warming condition can lead to an increasing SST trend. Although climate mode analysis from the CMIP6 revealed that the recent warming trend in the NTPO can be well explained by anthropogenic activity, the model bias can mask the current internal variability and lead to the wrong attribution (Seager et al. 2019), especially for the biogeochemical components which suffered from significant model biases relative to the observation (Lim et al. 2018). Therefore, a detailed analysis of climate model (or ESMs) simulations and attribution of model bias can contribute to revealing greenhouse warming effects on the recent persistent warming events.

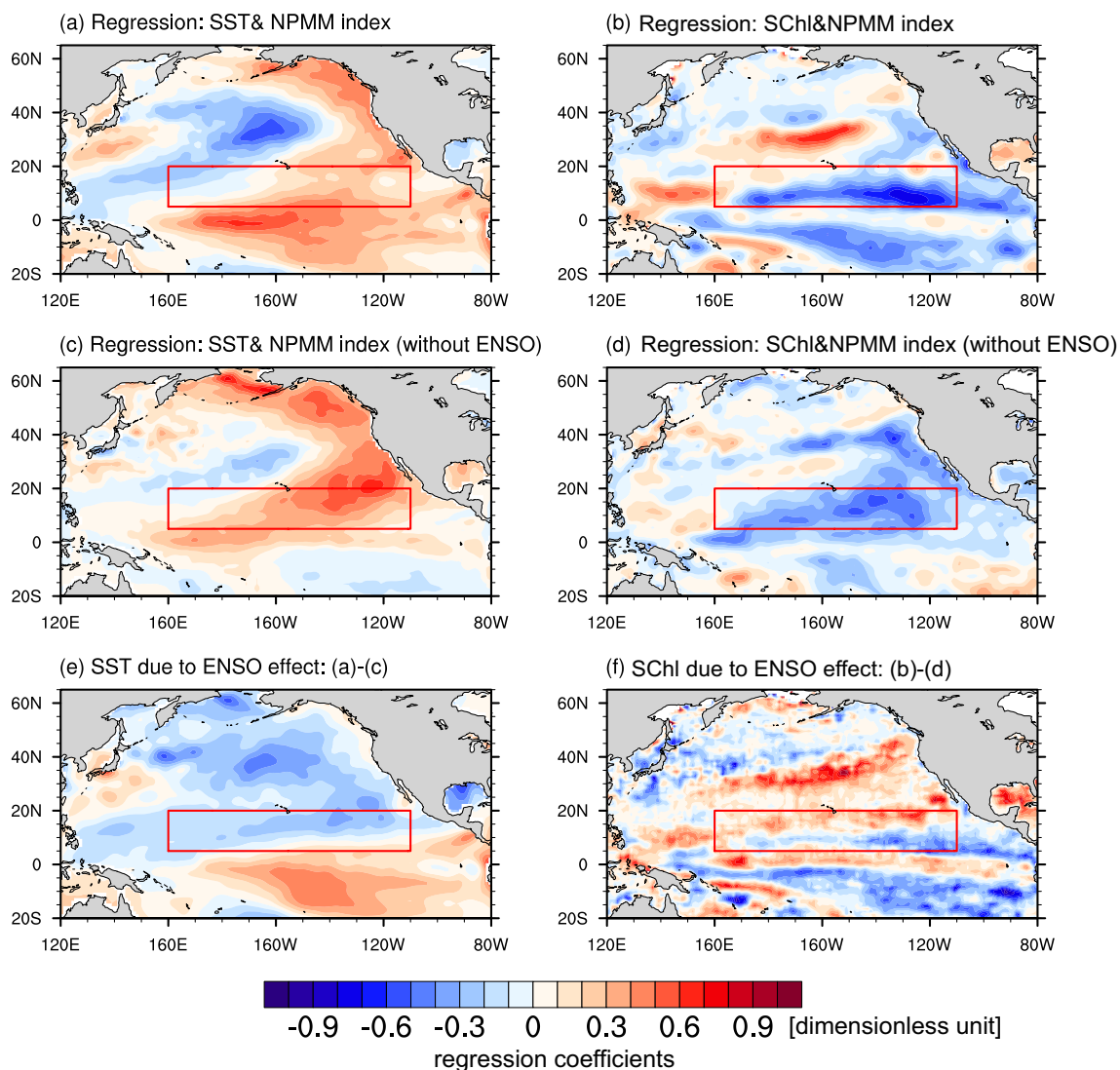


Fig. 13 Regression map of SST anomalies (a) and SChl (b) during MAM (1) onto the NPMM JFM index with ENSO impact being retained. c, d are the same as in a, b, but for the impact of ENSO which is removed by subtracting the linear regression map of the

SST (or SChl) onto Niño3.4 D(0)JF(1) index. e, f are the same as in a, b but for Niño3.4 D(0)JF(1) index. The SST and SChl used for regression analysis are based on the observational data from NOAA ERSSTv5 and GlobColor Project, respectively

7 Summary

In this study, we found that during 2013–2020, the NTPO experienced persistent surface warming, a low surface chlorophyll (SChl), and a transition from carbon source to sink. By analyzing observational data and multi-climate model simulations, we found that the interactions between the North Pacific meridional mode (NPMM) and multi-year El Niño events jointly led to this unusually long-lasting compound event (Fig. 16). The warm phase of NPMM first

excited an anticyclonic circulation in the NTPO, which subsequently induced surface warming in the western sector (160° E–150° W) through the wind-evaporation-SST feedback and suppressed the thermocline in the eastern sector (150° W–110° W) through Ekman suction, corresponding to a decrease in SChl. Secondly, the NPMM (+) impacts can trigger El Niño events during the subsequent winter, which further maintained the negative anomalies in SChl by weakening the surface current. By this loop, two persistent El Niño events (2014–2016 and 2018–2020) happened

Fig. 14 Relationship of observed SChI anomalies in NTPO during MAM and NPMM with SST during JFM (a) and Niño34 SST during D(0)JF from 1998 to 2020 (b); red and green dots denote El Niño and La Niña years, respectively. The SST and SChI used for analysis are based on the observational data from NOAA ERSSTv5 and GlobColor Project, respectively

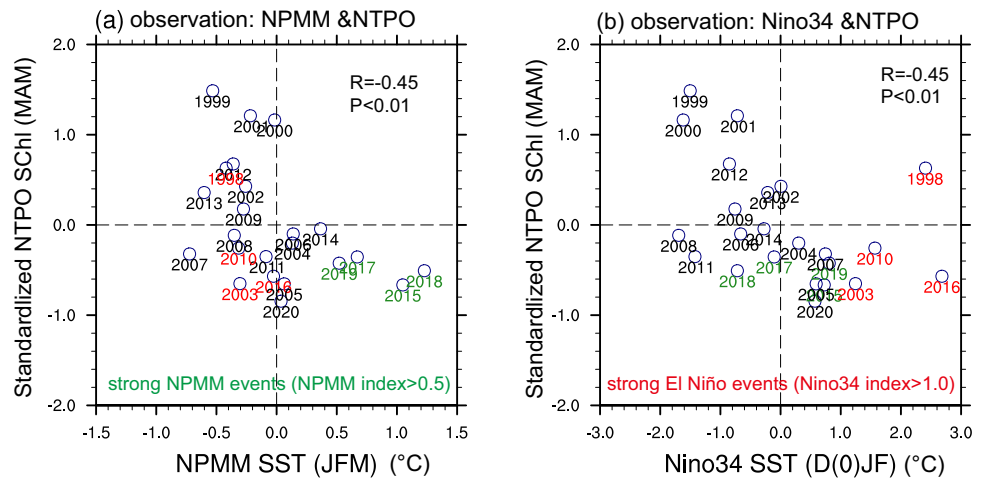
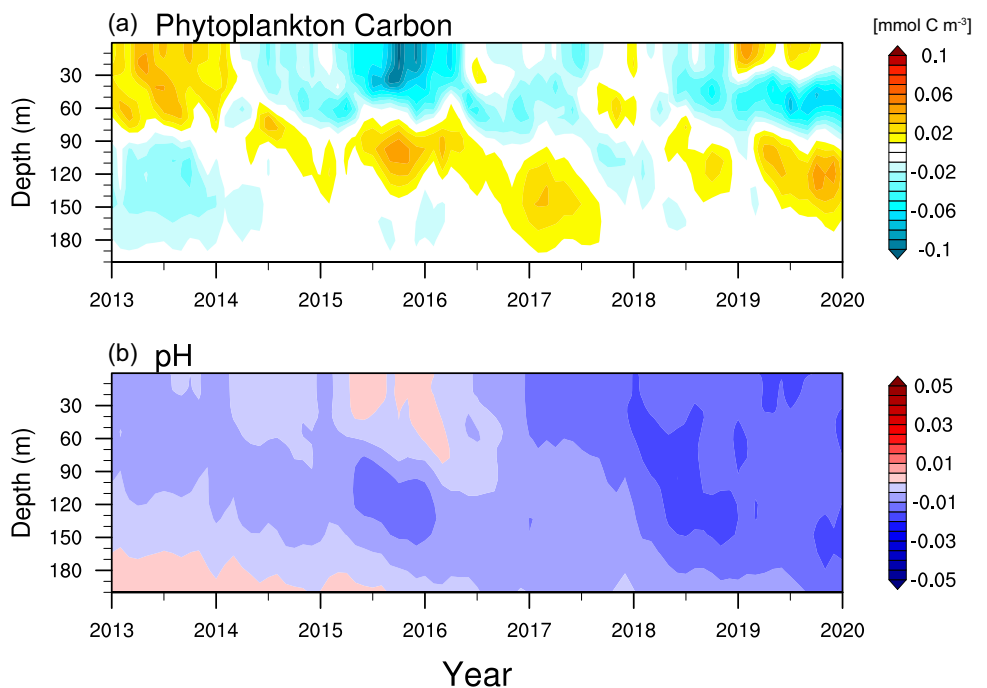


Fig. 15 Time-depth (0–200 m) section for phytoplankton carbon (a) and pH (b) anomalies averaged over the NTPO (5° N–20° N, 160° E–110° W) from January 2013 through December 2020. The datasets are from CMEMS biogeochemical hindcast simulations



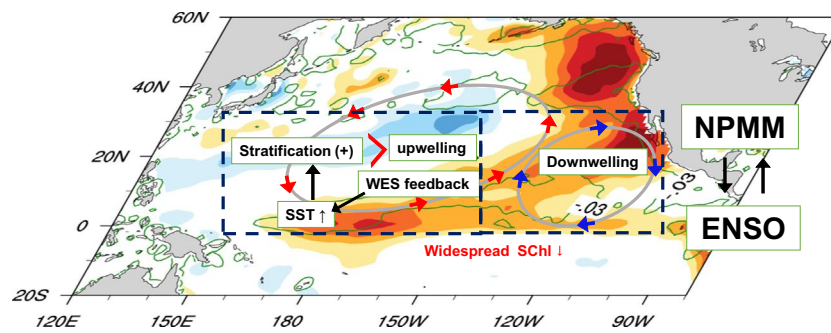


Fig. 16 Schematic illustration of the primary physical drivers responsible for the persistent warming and low SCHl. The warm phase of NPMM first excites an anticyclonic circulation in the NTPO, which subsequently induces surface warming in the western sector (160° E–150° W) through the wind-evaporation-SST (WES) feedback and suppresses the thermocline in the eastern sector (150° W–110° W) through Ekman suction, corresponding to a decrease in SCHl. Secondly, the NPMM (+) impacts can trigger El Niño events during the

subsequent winter, which further maintains the negative anomalies in SCHl by weakening the surface current. By this loop, two persistent El Niño events (2014–2016 and 2018–2020) happen in succession and subsequently pull down the decreasing trend in SCHl by 2020. The background picture is taken from observed SST (shaded) and SCHl (contours with the interval being 0.03 mg m⁻³) anomalies during MAM 2015

in succession and subsequently pulled down the decreasing trend in SCHl by 2020. Further heat budget analyses and OGCM experiments revealed that the net surface heat flux due to the NPMM significantly contributed to persistent warming. At the same time, the contribution from changes in the wind field was relatively small. These findings can help to illustrate the effects of extratropical-tropical interactions on the compound physical-biological extremes under the global warming scenario.

Supplementary Information The online version contains supplementary material available at <https://doi.org/10.1007/s00382-024-07184-4>.

Acknowledgements The authors wish to thank Hyung-Gyu Lim and another anonymous reviewer for their insightful comments that greatly helped improve the original manuscript.

Funding This work is supported by the National Natural Science Foundation of China (NSFC; Grant nos. 42030410 and 42006001), the Strategic Priority Research Program of the Chinese Academy of Sciences (Grant no. XDB42000000 (XDB42040100, XDB42040103)), Laoshan Laboratory (no. LSKJ202202402) and the Startup Foundation for Introducing Talent of NUIST.

Data availability We thank the GlobColor Project at the CMEMS website (<https://doi.org/10.48670/moi-00281>) supplied SCHl data, the National Oceanic and Atmospheric Administration (NOAA)/National Centers for Environmental Information (NCEI) provided ERSSTv5 data, (<https://www.ncei.noaa.gov/access/metadata/landing-page/bin/iso?id=gov.noaa.ncdc:C00927#Documentation>), NOAA/Physical Science Laboratory (PSL) provided GODAS data (<https://psl.noaa.gov/data/gridded/data.godas.html>), National Centers for Environmental Prediction (NCEP) (<https://psl.noaa.gov/data/gridded/data.ncep.reanalysis.html>) and ECMWF Reanalysis v5 (ERA5) provided atmospheric reanalysis data (<https://www.ecmwf.int/en/forecasts/dataset/ecmwf-reanalysis-v5>), Met Office provided EN4 data (<https://www.metoffice.gov.uk/hadobs/en4/>), Copernicus Marine Environment Monitoring Service (CMEMS) provided altimeter satellite gridded data and hindcast biogeochemical simulation data (<https://data.marine.copernicus.eu/products>), and Oregon State University provided net

primary productivity data (<https://sites.science.oregonstate.edu/ocean.productivity/>). We also thank the climate modeling groups (listed in Table S1) for producing and making available their model outputs, and the Earth System Grid Federation (ESGF) for archiving the CMIP6 data and providing access; CMIP6 outputs were downloaded from the ESGF-DOE/LLNL node by <https://esgf-node.llnl.gov/search/cmip6/>. We also thank the Max Planck Institute for Meteorology (MPI-M) for developing the Climate Data Operator (CDO) software version 1.6.9 at <http://mpimet.mpg.de/cdo>.

Declarations

Conflict of interest The authors declare no competing interests.

References

- Amaya DJ (2019) The Pacific meridional mode and ENSO: a review. *Curr Clim Chang Reports* 5:296–307. <https://doi.org/10.1007/s40641-019-00142-x>
- Amaya DJ, Miller AJ, Xie SP, Kosaka Y (2020) Physical drivers of the summer 2019 North Pacific marine heatwave. *Nat Commun* 11:1–9. <https://doi.org/10.1038/s41467-020-15820-w>
- Arteaga L, Pahlow M, Oschlies A (2014) Global patterns of phytoplankton nutrient and light colimitation inferred from an optimality-based model. *Global Biogeochem Cycles* 28:648–661. <https://doi.org/10.1002/2013GB004668>
- Aumont O, Bopp L (2006) Globalizing results from ocean in situ iron fertilization studies. *Global Biogeochem Cycles* 20:1–15. <https://doi.org/10.1029/2005GB002591>
- Aumont O, Ethé C, Tagliabue A et al (2015) PISCES-v2: an ocean biogeochemical model for carbon and ecosystem studies. *Geosci Model Dev* 8:2465–2513. <https://doi.org/10.5194/gmd-8-2465-2015>
- Behringer DW (2007) The global ocean data assimilation system (GODAS) at NCEP. Preprints, 11th symp. on integrated observing and assimilation systems for atmosphere, oceans, and land surface, San Antonio, TX, Amer. Meteor. Soc., 3.3. http://ams.confex.com/ams/87ANNUAL/techprogram/paper_119541.htm
- Browning TJ, Moore CM (2023) Global analysis of ocean phytoplankton nutrient limitation reveals high prevalence of

- co-limitation. *Nat Commun* 14:1–12. <https://doi.org/10.1038/s41467-023-40774-0>
- Browning TJ, Saito MA, Garaba SP et al (2023) Persistent equatorial Pacific iron limitation under ENSO forcing. *Nature*. <https://doi.org/10.1038/s41586-023-06439-0>
- Burger FA, Terhaar J, Frölicher TL (2022) Compound marine heatwaves and ocean acidity extremes. *Nat Commun* 13:4722. <https://doi.org/10.1038/s41467-022-32120-7>
- Cai W, Borlace S, Lengaigne M et al (2014) Increasing frequency of extreme El Niño events due to greenhouse warming. *Nat Clim Chang* 5:1–6. <https://doi.org/10.1038/nclimate2100>
- Cai W, Yang K, Wu L et al (2021) Opposite response of strong and moderate positive Indian Ocean Dipole to global warming. *Nat Clim Chang* 11:27–32. <https://doi.org/10.1038/s41558-020-00943-1>
- Chang P, Zhang L, Saravanan R et al (2007) Pacific meridional mode and El Niño–Southern oscillation. *Geophys Res Lett* 34:1–5. <https://doi.org/10.1029/2007GL030302>
- Chavez FP, Strutton PG, McPhaden MJ (1998) Biological-physical coupling in the central equatorial Pacific during the onset of the 1997–98 El Niño. *Geophys Res Lett* 25:3543–3546. <https://doi.org/10.1029/98GL02729>
- Chen H, Wang Y, Xiu P et al (2023) Combined oceanic and atmospheric forcing of the 2013/14 marine heatwave in the northeast Pacific. *Npj Clim Atmos Sci* 6:3. <https://doi.org/10.1038/s41612-023-00327-0>
- Cheng L, von Schuckmann K, Abraham JP et al (2022) Past and future ocean warming. *Nat Rev Earth Environ* 3:776–794. <https://doi.org/10.1038/s43017-022-00345-1>
- Christian JR, Verschell MA, Murtugudde R et al (2001) Biogeochemical modelling of the tropical Pacific Ocean. I: seasonal and interannual variability. *Deep Sea Res Part II Top Stud Oceanogr* 49:509–543. [https://doi.org/10.1016/S0967-0645\(01\)00110-2](https://doi.org/10.1016/S0967-0645(01)00110-2)
- Coralie P, Camille S, Julien P, Marie D (2019) Quality information document: global production centre GLOBAL_REANALYSIS_BIO_001_029
- Cronin MF, Pelland NA, Emerson SR, Crawford WR (2015) Estimating diffusivity from the mixed layer heat and salt balances in the North Pacific. *J Geophys Res Ocean* 120:7346–7362. <https://doi.org/10.1002/2015JC011010>
- Di Lorenzo E, Mantua N (2016) Multi-year persistence of the 2014/15 North Pacific marine heatwave. *Nat Clim Chang* 6:1042–1047. <https://doi.org/10.1038/nclimate3082>
- Ding R, Tseng Y, Di Lorenzo E et al (2022) Multi-year El Niño events tied to the North Pacific Oscillation. *Nat Commun* 13:3871. <https://doi.org/10.1038/s41467-022-31516-9>
- Doney SC, Ruckelshaus M, Emmett Duffy J et al (2012) Climate change impacts on marine ecosystems. *Ann Rev Mar Sci* 4:11–37. <https://doi.org/10.1146/annurev-marine-041911-111611>
- Duan J, Li Y, Cheng L et al (2023) Heat storage in the upper Indian ocean: the role of wind-driven redistribution. *J Clim* 36(7):2221–2242. <https://doi.org/10.1175/JCLI-D-22-0534.1>
- Gnanadesikan A, Anderson WG (2009) Ocean water clarity and the ocean general circulation in a coupled climate model. *J Phys Oceanogr* 39:314–332. <https://doi.org/10.1175/2008JPO3935.1>
- Good SA, Martin MJ, Rayner NA (2013) EN4: quality controlled ocean temperature and salinity profiles and monthly objective analyses with uncertainty estimates. *J Geophys Res Ocean* 118:6704–6716. <https://doi.org/10.1002/2013JC009067>
- Gruber N, Boyd PW, Frölicher TL, Vogt M (2021) Biogeochemical extremes and compound events in the ocean. *Nature* 600:395–407. <https://doi.org/10.1038/s41586-021-03981-7>
- Guan C, Wang X, Yang H (2023) Understanding the development of the 2018/19 Central Pacific El Niño. *Adv Atmos Sci* 40:177–185. <https://doi.org/10.1007/s00376-022-1410-1>
- Hersbach H, Bell B, Berrisford P et al (2020) The ERA5 global reanalysis. *Q J R Meteorol Soc* 146:1999–2049. <https://doi.org/10.1002/qj.3803>
- Hu S, Fedorov AV (2017) The extreme El Niño of 2015–2016 and the end of global warming hiatus. *Geophys Res Lett* 44:3816–3824. <https://doi.org/10.1002/2017GL072908>
- Huang B, Thorne PW, Banzon VF et al (2017) Extended reconstructed Sea surface temperature, Version 5 (ERSSTv5): upgrades, validations, and intercomparisons. *J Clim* 30:8179–8205. <https://doi.org/10.1175/JCLI-D-16-0836.1>
- Jia F, Cai W, Gan B et al (2021) Enhanced North Pacific impact on El Niño/Southern Oscillation under greenhouse warming. *Nat Clim Chang*. <https://doi.org/10.1038/s41558-021-01139-x>
- Lee K-W, Yeh S-W, Kug J-S, Park J-Y (2014) Ocean chlorophyll response to two types of El Niño events in an ocean-biogeochemical coupled model. *J Geophys Res Ocean* 119:933–952. <https://doi.org/10.1002/2013JC009050>
- Lim HG, Park JY, Kug JS (2018) Impact of chlorophyll bias on the tropical Pacific mean climate in an earth system model. *Clim Dyn* 51:2681–2694. <https://doi.org/10.1007/s00382-017-4036-8>
- Lim H, Dunne JP, Stock CA et al (2022) Oceanic and atmospheric drivers of post-El-Niño chlorophyll rebound in the equatorial Pacific. *Geophys Res Lett*. <https://doi.org/10.1029/2021GL096113>
- Liu H, Nie X, Cui C, Wei Z (2023) Compound marine heatwaves and low sea surface salinity extremes over the tropical Pacific Ocean. *Environ Res Lett* 29:465705. <https://doi.org/10.1088/1748-9326/acd0c4>
- Madec G (2014) “NEMO ocean engine” (Draft edition r5171) Note du Pôle de modélisation de l’Institut Pierre-Simon Laplace
- Maes C (2000) Salinity variability in the equatorial Pacific Ocean during the 1993–98 period. *Geophys Res Lett* 27:1659–1662. <https://doi.org/10.1029/1999GL011261>
- Maritorena S, d’Andon OHF, Mangin A, Siegel DA (2010) Merged satellite ocean color data products using a bio-optical model: characteristics, benefits and issues. *Remote Sens Environ* 114:1791–1804. <https://doi.org/10.1016/j.rse.2010.04.002>
- Messié M, Chavez FP (2013) Physical-biological synchrony in the global ocean associated with recent variability in the central and western equatorial Pacific. *J Geophys Res Ocean* 118:3782–3794. <https://doi.org/10.1002/jgrc.20278>
- Murtugudde RG, Signorini SR, Christian JR et al (1999) Ocean color variability of the tropical Indo-Pacific basin observed by SeaWiFS during 1997–1998. *J Geophys Res Ocean* 104:18351–18366. <https://doi.org/10.1029/1999jc900135>
- Murtugudde R, Beauchamp J, McClain CR et al (2002) Effects of penetrative radiation of the upper tropical ocean circulation. *J Clim* 15:470–486. [https://doi.org/10.1175/1520-0442\(2002\)015%3c0470:EOPROT%3e2.0.CO;2](https://doi.org/10.1175/1520-0442(2002)015%3c0470:EOPROT%3e2.0.CO;2)
- Nakamura Y, Oka A (2019) CMIP5 model analysis of future changes in ocean net primary production focusing on differences among individual oceans and models. *J Oceanogr* 75:441–462. <https://doi.org/10.1007/s10872-019-00513-w>
- Oliver ECJ, Benthuisen JA, Bindoff NL et al (2017) The unprecedented 2015/16 Tasman Sea marine heatwave. *Nat Commun* 8:16101. <https://doi.org/10.1038/ncomms16101>
- Park J-Y, Kug J-S, Park J et al (2011) Variability of chlorophyll associated with El Niño–Southern Oscillation and its possible biological feedback in the equatorial Pacific. *J Geophys Res* 116:C10001. <https://doi.org/10.1029/2011JC007056>
- Radenac M-H, Léger F, Singh A, Delcroix T (2012) Sea surface chlorophyll signature in the tropical Pacific during eastern and central Pacific ENSO events. *J Geophys Res Ocean*. <https://doi.org/10.1029/2011JC007841>
- Schmeisser L, Bond NA, Siedlecki SA, Ackerman TP (2019) The role of clouds and surface heat fluxes in the maintenance of the 2013–2016 Northeast Pacific marine heatwave. *J Geophys Res Atmos* 124:10772–10783. <https://doi.org/10.1029/2019JD030780>

- Seager R, Cane M, Henderson N et al (2019) Strengthening tropical Pacific zonal sea surface temperature gradient consistent with rising greenhouse gases. *Nat Clim Chang* 9:517–522. <https://doi.org/10.1038/s41558-019-0505-x>
- Shchepetkin AF, McWilliams JC (2005) The regional oceanic modeling system (ROMS): a split-explicit, free-surface, topography-following-coordinate oceanic model. *Ocean Model* 9:347–404. <https://doi.org/10.1016/j.ocemod.2004.08.002>
- Shi W, Wang M (2014) Satellite-observed biological variability in the equatorial Pacific during the 2009–2011 ENSO cycle. *Adv Sp Res* 54:1913–1923. <https://doi.org/10.1016/j.asr.2014.07.003>
- Smale DA, Wernberg T, Oliver ECJ et al (2019) Marine heatwaves threaten global biodiversity and the provision of ecosystem services. *Nat Clim Chang* 9:306–312. <https://doi.org/10.1038/s41558-019-0412-1>
- Smith KE, Burrows MT, Hobday AJ et al (2023) Biological impacts of marine heatwaves. *Ann Rev Mar Sci* 15:1–27. <https://doi.org/10.1146/annurev-marine-032122-121437>
- Tian F, Zhang R-H, Wang X (2019) Factors affecting interdecadal variability of air–sea CO₂ fluxes in the tropical Pacific revealed by an ocean physical–biogeochemical model. *Clim Dyn* 53(7–8):3985–4004. <https://doi.org/10.1007/s00382-019-04766-5>
- Tian F, Zhang R-H, Wang X (2021a) Coupling ocean–atmosphere intensity determines ocean chlorophyll-induced SST change in the tropical Pacific. *Clim Dyn* 56:3775–3795. <https://doi.org/10.1007/s00382-021-05666-3>
- Tian F, Zhang R-H, Wang X, Zhi H (2021b) Rectified effects of interannual chlorophyll variability on the tropical Pacific climate revealed by a hybrid coupled physics–biology model. *J Geophys Res Ocean*. <https://doi.org/10.1029/2021JC017263>
- Turk D, Meinen CS, Antoine D et al (2011) Implications of changing El Niño patterns for biological dynamics in the equatorial Pacific Ocean. *Geophys Res Lett*. <https://doi.org/10.1029/2011GL049674>
- Vimont DJ, Wallace JM, Battisti DS (2003) The seasonal footprinting mechanism in the Pacific: implications for ENSO*. *J Clim* 16:2668–2675. [https://doi.org/10.1175/1520-0442\(2003\)016%3c2668:TSFMIT%3e2.0.CO;2](https://doi.org/10.1175/1520-0442(2003)016%3c2668:TSFMIT%3e2.0.CO;2)
- Zhan W, Zhang Y, He Q, Zhan H (2023) Shifting responses of phytoplankton to atmospheric and oceanic forcing in a prolonged marine heatwave. *Limnol Oceanogr*. <https://doi.org/10.1002/lno.12388>
- Zhang R-H, Busalacchi AJ, Wang X et al (2009) Role of ocean biology-induced climate feedback in the modulation of El Niño–Southern Oscillation. *Geophys Res Lett*. <https://doi.org/10.1029/2008GL036568>
- Zhang R-H, Tian F, Zhi H et al (2019) Observed structural relationships between ocean chlorophyll variability and its heating effects on the ENSO. *Clim Dyn* 53(9–10):5165–5186. <https://doi.org/10.1007/s00382-019-04844-8>
- Zhang R-H, Zhou G, Zhi H et al (2022) Salinity interdecadal variability in the western equatorial Pacific and its effects during 1950–2018. *Clim Dyn*. <https://doi.org/10.1007/s00382-022-06417-8>
- Zheng F, Zhang RH (2012) Effects of interannual salinity variability and freshwater flux forcing on the development of the 2007/08 La Niña event diagnosed from Argo and satellite data. *Dyn Atmos Ocean* 57:45–57. <https://doi.org/10.1016/j.dynatmoce.2012.06.002>
- Zhi H, Lin P, Zhang RH et al (2019) Salinity effects on the 2014 warm “Blob” in the Northeast Pacific. *Acta Oceanol Sin* 38:24–34. <https://doi.org/10.1007/s13131-019-1450-2>

Publisher's Note Springer Nature remains neutral with regard to jurisdictional claims in published maps and institutional affiliations.

Springer Nature or its licensor (e.g. a society or other partner) holds exclusive rights to this article under a publishing agreement with the author(s) or other rightsholder(s); author self-archiving of the accepted manuscript version of this article is solely governed by the terms of such publishing agreement and applicable law.